Journal of Inflammation Research

Dovepress
Taylor & Francis Group

Open Access Full Text Article

ORIGINAL RESEARCH

The Inhibitory Effect of the Active Ingredients in the Bushen Huoxue Formula on the IL-17A Signaling Pathway and Its Alleviating Effect on Osteoarthritis

Xuan Wang[1,*], Yunheng Zhang[1,*], Xin Chang[1], Xiaodong Wen[1], Feng Tian[1], Hanjie Yu[2], Yi Li[1]

[1]Department of Foot and Ankle Surgery, Honghui Hospital, Xi'an Jiaotong University, Xi'an, People's Republic of China; [2]Laboratory for Functional Glycomics, College of Life Sciences, Northwest University, Xi'an, People's Republic of China

*These authors contributed equally to this work

Correspondence: Yi Li, Email footankle08@126.com

Objective: Osteoarthritis (OA) stands as a prevalent degenerative disease worldwide. Despite the demonstrated therapeutic efficacy of the Bushen Huoxue formula (BSHXF) in treating OA, its underlying mechanism remains elusive. Network pharmacology is commonly employed for investigating drug–disease associations and processes. In this study, we employed network pharmacology alongside in vitro and in vivo experiments to elucidate the molecular mechanism by which BSHXF treats OA.

Methods: Based on the TCMSP database, active components of BSHXF were screened, and OA-related targets were retrieved from GeneCard and DisGeNET to construct a "component-target-pathway" network using Cytoscape. Core target functions and pathways (KEGG/GO) were analyzed through STRING and Metascape, while component-target binding affinity was validated via Autodock. For in vitro experiments, an IL-1β-induced chondrocyte inflammation model was established, and key protein expression was detected by Western blot and immunofluorescence. For in vivo experiments, an OA model was created by medial meniscectomy of the knee joint in rats, and therapeutic efficacy was assessed using histological staining and micro-CT.

Results: This study screened 89 active ingredients of BSHXF and identified 189 common targets. Network pharmacological analysis revealed luteolin and tanshinone IIA as the most crucial active ingredients in treating OA with BSHXF. The potential mechanisms of action for BSHXF in OA treatment involve inflammation inhibition, immune function regulation, and resistance to oxidative stress, with a significant regulatory role played by the IL-17 signaling pathway. Molecular docking results demonstrated luteolin's strong binding affinity to key targets such as B-cell lymphoma 2 (Bcl-2), Matrix metalloproteinase-9 (Mmp-9), and IL-6.In vitro experiments demonstrated that BSHXF significantly suppressed IL-1β-induced inflammatory responses in chondrocytes, downregulating IL-17A expression ($p < 0.05$), reducing the expression of MMP-9 ($p < 0.05$) and IL-6 ($p < 0.05$), and inhibiting apoptosis. Additionally, in vivo experiments revealed that the high-dose BSHXF group (150 mg/kg) markedly alleviated cartilage damage in OA rats, with OARSI scores significantly decreased compared to the model group ($p < 0.05$). Micro-CT analysis showed that BSHXF inhibited osteophyte formation and ameliorated OA pathological conditions.

Conclusion: BSHXF has the potential to alleviate OA by suppressing inflammation, inhibiting cartilage apoptosis and hindering extracellular matrix degradation via the IL-17 signaling pathway. Our study elucidated the molecular mechanisms underlying the therapeutic effects of BSHXF on OA, thus highlighting its further research implications as a novel drug candidate.

Keywords: osteoarthritis, Bushen Huoxue formula, pharmacological mechanism, network pharmacology, experimental verification

Introduction

Osteoarthritis (OA) is a degenerative disease that affects the health of middle-aged and older adults worldwide, with its prevalence significantly increasing over recent decades owing to the trend of population aging and the escalating issue of obesity. This trend has significantly compounded the healthcare burden worldwide.[1] An increasing number of countries

Received: 15 November 2024
Accepted: 8 May 2025
Published: 21 May 2025

© 2025 Wang et al. This work is published and licensed by Dove Medical Press Limited. The full terms of this license are available at https://www.dovepress.com/terms.php and incorporate the Creative Commons Attribution – Non Commercial (unported, v4.0) License (http://creativecommons.org/licenses/by-nc/4.0/). By accessing the work you hereby accept the Terms. Non-commercial uses of the work are permitted without any further permission from Dove Medical Press Limited, provided the work is properly attributed. For permission for commercial use of this work, please see paragraphs 4.2 and 5 of our Terms (https://www.dovepress.com/terms.php).

are directing attention towards the prevention and treatment of OA, driven by the realization that patients with OA face higher risks of all-cause mortality, especially cardiovascular diseases, compared to the general population. This excess mortality is closely associated with the degree of disability.[2–4] OA affects multiple joints throughout the body, most commonly the knees, hands, hips, and spine. Although clinical manifestations vary significantly among individuals, joint damage remains the hallmark pathological feature of the disease.[5,6] The etiology of OA typically falls into two categories: primary and secondary. Primary OA is the result of multiple risk factors contributing to its development, including obesity, comorbidities, occupation, physical activity, biological factors, and dietary exposures. Secondary OA risk factors predominantly include trauma, congenital malformations, and surgical sequelae.[7,8] The pathogenesis of knee OA remains unclear, with current domestic and international research focusing on the imbalance theory involving matrix metalloproteinases (MMPs) and tissue inhibitors of matrix metalloproteinases (TIMPs). When OA occurs, chondrocytes abnormally secrete MMPs, affecting the production of TIMPs and leading to the acceleration of matrix degradation. Moreover, some of the cytokines, such as tumor necrosis factor alpha (TNF-α) and interleukin 1 (IL-1), are involved in the regulation of this process, directly or indirectly activating signal pathways such as Transforming Growth Factor-beta (TGF-β), nuclear factor κB (NF-κB), and MAPK, which provide insights into the pathogenesis of OA.[9–11] Additionally, following the activation of multiple inflammatory signaling pathways, numerous inflammatory factors can be detected in joint fluid and serum.[12] OA is a whole-joint disease, and its pathological features include not only changes in the biomechanical behavior of chondrocytes, but also lesions in all tissues within the joint, such as meniscus degeneration, inflammation and fibrosis of the infrapatellar fat pad, and inflammation and fibrosis of the synovium.[13–15] Together, these pathological changes lead to structural destruction and dysfunction of the joint. These features, supplemented by imaging modalities such as X-ray, ultrasound, and magnetic resonance imaging, can aid in the diagnosis of OA.[16] In addition, clinical staging of OA typically adheres to the criteria established by the American Academy of Orthopedic Surgeons (AAOS) which classifies OA into grades 0 through 4, with grade 0 indicating normality and grade 4 representing the most severe manifestation.[17] Inflammation exacerbates the progression of OA, as elevated systemic and local inflammatory cytokines promote cartilage degradation. Antigens from damaged joints further trigger inflammation through the activation of inflammatory vesicles. Moreover, inflammation and OA alter and regulate B and T lymphocyte populations, suggesting potential pathogenic pathways that could aid in identifying potential therapeutic targets for OA.[18,19] Currently, treatments for OA primarily aim to reduce symptoms, improve function, and delay disease progression. These treatments include pharmacological, physiological, and surgical interventions.[20,21] While most of these interventions effectively alleviate the symptoms of OA, they do not fundamentally change the development of the disease, ie, chronic inflammation. Although non-selective Non-steroidal anti-inflammatory drugs (NSAIDs) can suppress inflammation, they are associated with gastrointestinal toxicity and can lead to dyspepsia, gastritis, and gastric ulcers.[22] In the early stages of OA, interventions such as autologous chondrocyte implantation (ACI), matrix-induced autologous chondrocyte implantation (MACI), and microfracture surgeries are viable options. However, these procedures entail varying degrees of risk, including ethical concerns associated with stem cell sources.[23,24] For patients with end-stage OA, arthroplasty is recommended; however, it is associated with deep infection and deep vein thrombosis.[18] Therefore, there is an urgent need to identify effective treatment options with fewer adverse effects. Thus, in addition to medication and surgery, other treatment modalities for OA, including nutritional supplements and traditional Chinese medicine (TCM),[25] are gaining attention. However, the effectiveness and safety of these therapeutic approaches require further research and validation.

TCM boasts a rich historical legacy in treating OA and has made significant progress in the field of medicine, presenting promising potential as a complementary or alternative therapy for OA. In addition, TCM interventions offers the advantages of good prognosis, cost-effectiveness, and a reduced incidence of adverse symptoms, rendering its application in the treatment of OA safer and more reliable.[26] BSHXF comprises five principal medicinal herbs: *Rehmannia glutinosa, Salvia miltiorrhiza, Morinda officinalis, Cymbidium goeringii*, and *Aconitum carmichaelii*, This formula has been employed in the treatment of various systemic diseases for many years.[27,28] Particularly in the context of OA treatment, the utilization of BSHXF has emerged as a novel therapeutic option; however, the precise molecular mechanism underlying BSHXF's efficacy in OA treatment remains unclear. In recent years, many scholars have endeavored to elucidate this aspect. For example, Ping- Er Wang et al[29] explored the effect of BSHXF on chondrocyte degradation in a mouse model of OA and found that BSHXF could inhibit chondrocyte degradation by downregulating

the expression of MMP13 through the TGF-β signaling pathway. Hui-Hui Xu et al,[30] through pharmacological analysis, predicted potential targets of BSHXF for OA treatment. Subsequent in vivo experiments validated that BSHXF significantly inhibits chondrocyte apoptosis and suppresses the expression of Cysteine protease-3 (CASP3), CASP8, and CASP9. In addition, to further investigate the mechanism of action of BSHXF on OA, comprehensive investigations have been conducted on the primary active components of BSHXF. These studies have revealed their capability to inhibit the expression of IL-1β and to downregulate MMP2 and Collagen Type I (COL1), which play an antagonistic role in the development of OA.[31] A randomized controlled trial conducted by Zhan et al,[32] demonstrated that the combination of Bushen Huoxue Formula (BSHXF) and lumbar traction therapy exhibited significant improvements in pain intensity (VAS), functional disability (ODI), and lumbar range of motion in patients with chronic degenerative low back pain (DLBP). The therapeutic benefits persisted through 3-month follow-up assessments, with a markedly superior clinical efficacy rate observed in the intervention group compared to controls (32.35% vs 3.13%, $P<0.05$). No adverse events were reported, indicating favorable safety profiles for this integrated treatment modality. However, despite these preliminary studies, the precise mechanisms underlying the intricate chemical interactions within herbal formulations and the complex biological processes of human diseases remain elusive. Additionally, we are confronted with unanswered questions regarding the latent associations and targeted actions of BSHXF in OA.

Based on the theory of systems biology,[33] network pharmacology is a new and effective method to elucidate the molecular mechanism of drugs by identifying specific targets for network analysis, which can systematically analyze the regulatory topology of multi-components in traditional Chinese medicine compound acting synergistically on disease-related signaling networks. Molecular docking is an effective computer modeling technique. Through computer simulation, calculation and analysis, it can realize the docking and analysis of small molecular weight structures and related disease targets, so as to screen the material basis of pharmacodynamics. This method enables the rapid and efficient discovery of novel bioactive lead compounds from databases.[34] The core scientific hypothesis of this study is that multiple active ingredients in BSHXF formula can simultaneously target and regulate key target groups in the pathological process of OA (including inflammatory response, chondrocyte apoptosis, extracellular matrix degradation and other biological processes) through a synergistic mechanism, forming a multi-dimensional intervention network therapeutic effect. At the same time, an in vitro cell model and animal experiments were established for biological verification.

Materials and Methods

Acquisition of BSHXF and OA-Related Targets

In the Traditional Chinese Medicine Systematic Pharmacology Database and Analysis Platform (TCMSP) (https://old.tcmsp-e.com/), the ingredients of BSHXF were searched, including "Salvia miltiorrhiza" "Rehmannia" "Aconite" "Morinda morinda" and "Xianmao". The potential targets of BSHXF were identified employing specific screening criteria: oral bioavailability ≥30% and drug similarity ≥0.18. Human gene abbreviations corresponding to each target were determined using the UniProt database (https://www.UniProt.org/UniProt/).[35] For OA, relevant targets were retrieved from the GeneCards database (https://www.Genecards.org/) and the DisGeNET database (www.disgenet.org/search), followed by selection.[36,37]

BSHXF–OA Target Protein Interaction Network

BSHXF ingredients and OA target points were intersected, and a Venn diagram was generated to illustrate this overlap. The intersected target points were subsequently entered into the STRING website, specifying the selection criteria as "Homosapiens" and establishing a minimum interaction score threshold of 0.4. The protein–protein interaction (PPI) network diagram was then downloaded and imported into Cytoscape 3.7.2 to facilitate the visual analysis of the protein interactions.[38] Topological analysis of the interaction network was performed using the CytoNCA plug-in, whereby nodes exhibiting high degree centrality were identified as topologically important nodes in the network.[39] Based on these topological analysis results, potential targets were further screened from the intersection targets between active ingredients and diseases. The size of nodes was positively indicative of their respective correlations.

Active Ingredients–Common Targets–OA Regulatory Network

To visually elucidate the significance of various active ingredients, we utilized Cytoscape 3.7.2 for the construction of an active ingredient–target map. The topological analysis of the interaction network was performed using the CytoNCA plug-in, facilitating the acquisition of node connectivity.

Gene Ontology (GO) Biological Function and Kyoto Encyclopedia of Genes and Genomes (KEGG) Analysis

To elucidate the roles of target proteins in gene function and signaling pathways, we conducted a comprehensive GO analysis utilizing the annotated, visualized, and integrated discovery database Metascape (https://metascape.org). The functional enrichment analysis of GO and KEGG pathways revealed the significant impact of BSHXF on specific pathways during the treatment of OA.[40]

Molecular Docking

To assess the reliability of interactions between the targets and to elucidate the precise binding mode, we employed core genes as molecular receptors and conducted molecular docking analyses using luteolin and tanshinone IIA, the principal active ingredients of BSHXF. The original files (mol2 format) for luteolin and tanshinone IIA were downloaded from the PubChem database (https://pubchem.ncbi.nlm.nih.gov/), while the 3D structures of the target proteins were downloaded from the RCSB PDB (http://www.rcsb.org/) and saved in the PDB format. Subsequently, We set up the active compound protein file in AutoDock4 . This process involves the removal of water molecules and their replacement with hydrogen atoms, which are then saved in PDBQT format. The removal of water molecules and small molecule ligands from the target protein structure was carried out using PyMOL 2.2.0 software (https://pymol.org/). The resulting data was then imported into AutoDockTools 1.1.2 for dehydration reaction and hydrogenation preprocessing, and saved in PDBQT format. To assess the adhesion and activity of the target and drug molecules, molecular docking was performed using AutoDock Vina 1.1.2. The Local Search Algorithms algorithm was selected, with the energy parameters and step size parameters set to their default values. The binding energies of the molecules were analyzed, and the conformation with the lowest binding energy was chosen. Additionally, the formation of hydrogen bonds was observed. Finally, the images were refined using PyMOL 2.2.0.

Reagents and Antibodies

Luteolin (50 mg, HPLC≥98%) and Tanshinone IIA (50 mg, HPLC≥98%) were sourced from Sparkjade (Shandong, China), while IL-1β (50 μg, purity >95% by SDS-PAGE) was obtained from ABclonal(Wuhan, China). The 0.25% trypsin, CCK-8 kit, cell counting reagent, and Hoechst 33342 staining kit were purchased from Bitian (Jiangsu, China). The C28 cell line, fetal bovine serum (FBS), DMM/F12 medium, and Phosphate-Buffered Saline (PBS) were sourced from Zhongqiao Xinzhou (Shanghai, China). Annexin V-Fluorescein isothiocyanate (FITC) /propidium iodide (PI) apoptosis staining kit was acquired from Bode (Wuhan, China). Calcein acetoxymethyl ester (Calcein-AM) /PI Live/Dead Cell Double Staining Kit Purchased from ServiceBio (Wuhan, China). Primary antibodies targeting MMP-9, caspase 3, Bcl-2, and GAPDH, and enzyme-linked immunosorbent assay (ELISA) kits for IL-1, TNF-α, and IL-6 were obtained from Boster (Wuhan, China). The CALCEFIN-AM/PI Live/Dead cell double stain kit and antibodies against IL-17A, Actin alpha 1 (ACT1), TNF-α, cyclooxygenase (COX-2), and MMP-1 were purchased from ServiceBio (Wuhan, China).

Cell Culture

The medium was aspirated from the original culture bottle, and the cells were subsequently washed twice with PBS buffer. They were then digested for 2 min using 1–2 mL of pancreatic enzyme containing 0.25% ethylenediaminetetraacetic acid (EDTA). The digestion process was monitored under a microscope until the cell edges became reduced and detached from the substrate, indicating the removal of pancreatic enzymes. Subsequently, 6–8 mL of complete medium was added to gently dislodge the cell layer. A portion of the resulting cell suspension was transferred to a new T-25

bottle, while appropriate complete medium was added for further incubation in a culture chamber. Culture medium was periodically replaced, and when the cell density reached 70–80%, passage or freeze storage procedures were performed.

Establishment of OA Cell Model and Detection of Vitality Value

We established an OA cell model using IL-1β and assessed the cytotoxicity of two active ingredients on these cells. Chondrocytes ($5 \times 10^3/cm^2$) were seeded in 96-well plates and incubated at 37 °C for 24 h. Subsequently, the cells were treated with varying concentrations of luteolin (0, 5, 10, 20, and 50 μM) and tanshinone IIA (0, 5, 10, 20, and 50 μM). To quantitatively assess cell viability at a specific time point, we added CCK-8 reagent (10 μL) to each well, followed by incubation at 37 °C for 2 h. The optical density (OD) was then measured at a wavelength of 450 nm using an automated enzyme labeler (Thermo Fisher,America). The OD value was directly proportional to cell activity. Following determination of the effective concentration of the active ingredient(s), IL-1β (30 ng/mL) was introduced to each well, followed by an additional 24-h treatment period. Subsequently, different concentrations of luteolin (0, 5, and 10 μM) and tanshinone IIA (0, 5, 10, and 20 μM) were administered, with treatment durations of 12, 24, and 48 h, respectively, while monitoring cell viability. To evaluate cell viability during these specified time points, we added 10 μL of CCK-8 solution to each well, followed by incubation at 37 °C for 2 h. OD was then measured at a wavelength of 450 nm using an enzyme-labeled analyzer. All experiments were conducted in triplicate to ensure consistent results.

Cell Survival Assay

To assess the impact of drugs on cell survival, we subjected the cells to live/dead double staining using a Calcein-AM/PI kit, followed by examination under fluorescence microscopy (FV31S-SW, Olympus, Japan). The cells were subjected to the aforementioned treatment protocol, followed by digestion with 0.25% Trypsin-EDTA solution and subsequent harvesting of the cell suspension. Post-centrifugation at 800 *g* for 5 min, the cells were washed thrice with PBS and suspended in 1 mL Calcein AM/PI detection solution (2 μM/5 μg/mL) at a concentration of 1×10^6 cells/mL. Incubation was performed for 20 min in a light-free cell incubator before assessing the quantity of live and dead cells via fluorescence microscopy (excitation wavelength: 490 nm; emission wavelength: 500 nm). Living cells, labeled with Calcein-AM, exhibited green fluorescence, whereas dead cells, labeled with PI, emitted red fluorescence. All experiments were conducted in triplicate to ensure consistency.

Apoptosis Detection

To assess the extent of apoptosis in each group of chondrocytes, we stained the cells using an annexin V-FITC/PI apoptosis staining kit and subsequently analyzed them through flow cytometry. The specific protocol proceeded as follows: Post-treatment, cells were washed with PBS and subjected to digestion with EDTA-free trypsin digestion solution for 5 min. Subsequently, the cells were collected, centrifuged at 1200 *g* for 5 min to eliminate the supernatant, and suspended in 200 μL of binding buffer. Next, 4 μL of annexin V-FITC and 10 μL of PI were added to the cell suspension. Following a 10-min incubation period in the darkness, cell apoptosis was analyzed using a BD FACS Aria II SORP flow cytometer (BD Biosciences, USA) at 488 nm (BD FACSDiva v8.0). Additionally, the Hoechst 33342 staining method was employed to visualize cells under a fluorescence microscope. After replicating the aforementioned steps, Hoechst 33342 staining solution (10 μg/mL) was introduced to each well at room temperature and further incubated at 37 °C for 15 min within an incubator. Subsequently, cells were washed twice with PBS before their fluorescence signals were examined using fluorescence microscopy (excitation wavelength: 350 nm; emission wavelength: 461 nm). Images capturing the extent of cellular apoptosis were acquired and subjected to analysis. All experiments detailed herein were repeated three times to ensure consistent results.

Western Blot

To investigate the effects of luteolin and tanshinone IIA on IL-1B-induced chondrocytes, we extracted total protein from the cells using RIPA buffer supplemented with a protease inhibitor mixture. The protein concentration was determined via the Bicinchoninic Acid assay (BCA) method, and subsequently, 20 μg of total protein was isolated utilizing the SDS-PAGE method (10%). Subsequently, it was transferred onto a Polyvinylidene Fluoride(PVDF) membrane employing an

electrophoretic transfer device. The membrane was subsequently blocked with 5% skim milk at room temperature for 90 min before performing western blotting with corresponding primary and secondary antibodies. The procedural sequence is outlined as follows: The membrane was subjected to overnight incubation at 4 °C with a primary antibody (diluted at 1:1000), followed by three washes, each lasting 10 min, with TBST [0.05% Tween 20, 120 mmol/L Tris-HCl (pH 7.4) and 150 mmol/L NaCl] buffer on the subsequent day. Subsequently, the membrane was incubated with a secondary antibody (diluted at 1:5000) at room temperature for 90 min, followed by three additional 10 min washes with TBST buffer. Finally, the membranes were incubated with ECL chemiluminescent substrate for 5 minutes, followed by signal acquisition using a Bio-Rad chemiluminescence imaging system (Bio-Rad, USA) to detect protein expression. Quantitative analysis of protein bands was subsequently performed with Image Lab software (version6.1).

Immunofluorescence Staining

To investigate the impact of various treatments on chondrocytes, we performed immunofluorescence staining followed by observation using a scanning microscope (FV31S-SW, Olympus, Japan). The experimental protocol proceeded as follows: Chondrocytes were seeded onto 24-well plates at a density of 2×10^4 cells/well and incubated for 24 h. Subsequently, the cells were subjected to treatment with various agents, followed by fixation with 4% formaldehyde for 15 min, permeabilization with 0.2% Triton X-100 for 5 min, and blocking with 5% bovine serum albumin for 1 h. On the subsequent day, the respective primary antibody (diluted at a ratio of 1:200) was incubated overnight at 4 °C. The cells were then washed thrice with TBST for 10 min each. Afterwards, the appropriate fluorescent secondary antibody (diluted at a ratio of 1:500) was applied and incubated at room temperature in the absence of light for 1 h, followed by another three washes with TBST for 10 min each. Finally, 4',6-Diamidino-2-phenylindole (DAPI) stain (diluted at a ratio of 1:1000) was employed to label cell nuclei for 10 min, followed by two washes with PBS lasting 5 min each. Fluorescence signals emitted by the cells were quantitatively captured using fluorescence microscopy, with cellular morphology and fluorescence intensity systematically quantified and statistically analyzed through ImageJ software (version 2.9.0).

Preparation of Experimental Drugs

The BSHXF, comprised of *Rehmannia glutinosa* (24g),*Salvia miltiorrhiza* (24g), *Morinda officinalis* (12g),*Cymbidium goeringii* (10g), and *Aconitum carmichaelii* (12g), was provided by the Pharmacy Department of the Second Affiliated Hospital of Shaanxi University of Chinese Medicine. Dosage conversion from rats (250 g) to humans (60 kg) was performed in accordance with the "Laboratory Animal Pharmacology" guidelines, utilizing a conversion coefficient of 9.01. Consequently, the concentration of BSHXF administered to rats (82 g) was adjusted to 0.86 g/mL. To prepare the decoction, five doses of the aforementioned Chinese medicine were taken, and an equivalent amount of water (4200 mL) was added, allowing it to soak for 30 min. Subsequently, the mixture was boiled and simmered for an additional 30 min before being filtered using disinfection gauze, constituting the first decoction. This process was repeated with an additional fivefold amount of water (4200 mL) on the remaining residue to obtain a second decoction. Finally, both decoctions were combined and heated until the volume reduced to 500 mL, yielding the concentrated decoction of BSHXF, which was then stored at −80 °C in a refrigerator until further use.

Establishment of an OA Animal Model

We procured 40 male Sprague–Dawley (SD) rats, aged 8 weeks and weighing 250–300 g, from the Animal Center of Xi'an Jiaotong University School of Medicine (Xi'an, China).All animals were kept in the same environment (22±1 ° C, 50±5% humidity, 12-hour light-dark cycle), and all animal experiments followed the National Institutes of Health Guide for the Care and Use of Laboratory Animals. In the experiment, SD rats were fasted for 4 hours before surgery with free access to water to minimize the risk of vomiting and aspiration during anesthesia. Anesthesia was then administered via intraperitoneal injection of sodium pentobarbital at a dosage of 30–50 mg/kg. The modeling procedure was carried out once an appropriate depth of anesthesia was achieved.A sham surgery was performed on a group of 10 SD rats, involving solely an incision at the knee joint without excision of the medial meniscus, serving as a control group for comparative analysis. The remaining 30 rats underwent left knee medial meniscectomy to induce an OA model. Subsequently, 30 OA

model rats were stratified into 3 layers (10 rats per layer) based on knee joint swelling degree (measured by vernier caliper) and body weight (within ±5% range) at 24 hours post-operation to ensure balanced baseline characteristics. Within each layer, the 10 rats were then randomly assigned to OA group, low-dose group, and high-dose group (10 rats per group) using a random number table method. The sham surgery group (10 rats) was separately maintained and did not participate in the randomization process. After grouping was completed, oral gavage administration was initiated once daily for 12 consecutive weeks (Supplementary Figure 1). The operator performing the gavage was only aware of the cage numbers requiring administration each day and remained blinded to the corresponding drug codes for each group. Our study employed two dosage regimens: a low-dose formula (50 mg/kg) and a high-dose formula (150 mg/kg). Upon completion of the 12-week treatment period, all rats were euthanized by an overdose of sodium pentobarbital, and subsequent follow-up tests were conducted.

Elisa

The synovial fluid obtained from the left knee joint was collected at intervals of 4, 8, and 12 weeks post-treatment. Subsequent quantification was conducted using an ELISA kit to ascertain the concentrations of IL-1, IL-6, and TNF-α.

Micro-Computed Tomography (Micro-CT) Analysis

After immobilizing the knee joint overnight with 4% paraformaldehyde (PFA), we subjected it to a Micro-CT system scan lasting approximately 10 min at 43 kV and 43 μA. Subsequently, the scanned images of the knee joint were reconstructed and evaluated in three dimensions using ImageJ 2.9.0 and Amira 6.4.0. Based on this evaluation, quantitative morphometric indices were determined utilizing a 3D morphometric approach. These indices encompassed bone volume fraction (BV/TV, %), mean trabecular thickness (Tb.Th), mean trabecular number (Tb.N), and mean trabecular distance (Tb.Sp).

Histological Analysis

Cartilage tissues from the left knee joints of rats in each experimental group were harvested and subsequently fixed in 4% PFA for 24 h. Following fixation, the tissues were decalcified using 10% EDTA solution for 1 month. Subsequently, the cartilage tissues were dehydrated, embedded in paraffin, and sliced into 5-μm thick sections. Articular cartilage degradation in each knee joint was assessed via senna solid green O (S-O) staining, hematoxylin–eosin (H&E) staining, and toluidine blue (TB) staining, respectively. Changes in cartilage degradation were then analyzed employing the OA Research Society International (OARSI) scoring system. The cartilage damage depth, extent of damage, and bone redundancy were scored according to the OARSI criteria, which encompass six grades, ranging from very minor degeneration (0.5 point) to very severe degeneration (6 points). These scores were then aggregated to yield a total score reflecting the overall cartilage damage.[41] To minimize scoring bias, five professionally trained personnel independently conducted the assessments under blind conditions. This rigorous scoring procedure ensured the objectivity and accuracy of the assessments.

Statistical Analysis

The experiment was replicated at least three times. The results are presented as mean ± standard deviation (SD). The data were analyzed using SPSS 29.0 software (IBM Corp., Armonk, N.Y., USA, https://www.ibm.com/products/spss-statistics) and GraphPad Prism 9.0. (GraphPad Software, San Diego, CA, USA, http://www.graphpad.com) One-way analysis of variance (ANOVA) was employed for statistical examination. Non-parametric data (OARSI score) were analyzed using the Kruskal–Wallis H test. A p value of less than 0.05 was considered to indicate statistical significance.

Results

Screening the Active Ingredients of BSHXF

We conducted a search in the TCMSP database, applying filters for OB (≥30%) and DL (≥0.18), which led to the identification of a total of 118 active ingredients present in BSHXF. Subsequently, 29 inactive ingredients were excluded due to their lack of relevance or targeting, resulting in a final count of 89 active ingredients. For detailed information, please refer to Table 1.

Table 1 Active Ingredients of BSHXF

Compound code	Molecular Name	OB (%)	DL	Attribution
MOL002879	Dioctyl adipate	43.59	0.39	Morinda officinalis
MOL002883	Octadecenoic acid ethyl ester	32.4	0.19	Morinda officinalis
MOL000359	β-Sitosterol	36.91	0.75	Morinda officinalis
MOL006147	Alizarin-2-methyl ether	32.81	0.21	Morinda officinalis
MOL009495	2-Hydroxy-1,5-dimethoxy-6-methoxymethyl-9,10-anthraquinone	95.85	0.37	Morinda officinalis
MOL009496	1,5,7-Trihydroxy-6-methoxy-2-methoxymethylanthraquinone	80.42	0.38	Morinda officinalis
MOL009500	1,6-Dihydroxy-5-methoxy-2-methoxymethyl-9,10-anthraquinone	104.54	0.34	Morinda officinalis
MOL009504	1-Hydroxy-6-hydroxymethyl anthraquinone	81.77	0.21	Morinda officinalis
MOL009513	2-Hydroxy-1,8-dimethoxy-7-methoxymethylanthraquinone	112.3	0.37	Morinda officinalis
MOL009519	3,5-Dihydroxy-4,7-dimethoxydihydroflavonol	77.24	0.33	Morinda officinalis
MOL009524	3β,20®,5-Pentenyl-podophyllotoxin	36.91	0.75	Morinda officinalis
MOL009525	3β-24S-Butyl-5-pentenyl-cholestanol	35.35	0.82	Morinda officinalis
MOL009537	Americanin A	46.71	0.35	Morinda officinalis
MOL009562	Ohioensin-A	38.13	0.76	Morinda officinalis
MOL001601	1,2,5,6-Tetrahydrodanshensu	38.75	0.36	Salvia miltiorrhiza
MOL001659	Ergosterol	43.83	0.76	Salvia miltiorrhiza
MOL001771	Foeniculin-5-ene-3β-ol	36.91	0.75	Salvia miltiorrhiza
MOL001942	Isoimperatorin	45.46	0.23	Salvia miltiorrhiza
MOL002222	Taxifolin	36.11	0.28	Salvia miltiorrhiza
MOL002651	Dehydrosalvianolic acid II A	43.76	0.4	Salvia miltiorrhiza
MOL002776	Baicalin	40.12	0.75	Salvia miltiorrhiza
MOL000569	Dipalmitate	61.85	0.26	Salvia miltiorrhiza
MOL000006	Luteolin	36.16	0.25	Salvia miltiorrhiza
MOL006824	α-Amyloid peptide	39.51	0.76	Salvia miltiorrhiza
MOL007036	5,6-Dihydroxy-7-isopropyl-1,1-dimethyl-2,3-dihydrophen-4-one	33.77	0.29	Salvia miltiorrhiza
MOL007041	2-Isopropyl-8-methyl-3,4-phenanthraquinone	40.86	0.23	Salvia miltiorrhiza
MOL007045	3α-Hydroxydanshenone II.a	44.93	0.44	Salvia miltiorrhiza
MOL007050	2-(4-Hydroxy-3-methoxyphenyl)-5-(3-hydroxypropyl)-7-methoxy-3-benzofuranaldehyde	62.78	0.4	Salvia miltiorrhiza
MOL007051	6-Eugenyl-8-acetylshanzhiside methyl ester	46.69	0.71	Salvia miltiorrhiza
MOL007058	Formylated xanthine ketone	73.44	0.42	Salvia miltiorrhiza
MOL007059	3-β-Hydroxymethyl chloroacetate	32.16	0.41	Salvia miltiorrhiza
MOL007061	Toluquinone	37.07	0.36	Salvia miltiorrhiza
MOL007063	Zidanshen ether a	37.11	0.65	Salvia miltiorrhiza
MOL007064	Zidanshen ether b	110.32	0.44	Salvia miltiorrhiza
MOL007068	Zidanshen ethyl ester	62.24	0.41	Salvia miltiorrhiza
MOL007069	Zidanshen ethyl ester c	55.74	0.4	Salvia miltiorrhiza
MOL007071	Zidanshen ethyl ester f	40.31	0.46	Salvia miltiorrhiza
MOL007077	Perillalcohol	43.67	0.21	Salvia miltiorrhiza
MOL007079	Danshinal	52.47	0.45	Salvia miltiorrhiza
MOL007081	Danshenol B	57.95	0.56	Salvia miltiorrhiza
MOL007082	Danshenol A	56.97	0.52	Salvia miltiorrhiza
MOL007085	Salvilenone	30.38	0.38	Salvia miltiorrhiza
MOL007088	Cryptotanshinone	52.34	0.4	Salvia miltiorrhiza
MOL007093	Danshenquinone d	38.88	0.55	Salvia miltiorrhiza
MOL007094	Danshen lactone lactone	50.43	0.31	Salvia miltiorrhiza
MOL007098	Deoxy cryptoxanthin ketone	49.4	0.29	Salvia miltiorrhiza
MOL007100	Dihydrodanshen lactone	38.68	0.32	Salvia miltiorrhiza
MOL007101	Dihydrodanshenone I.	45.04	0.36	Salvia miltiorrhiza
MOL007105	Danshen lactone	68.27	0.31	Salvia miltiorrhiza

(*Continued*)

Table 1 (Continued).

Compound code	Molecular Name	OB (%)	DL	Attribution
MOL007107	C09092	36.07	0.25	Salvia miltiorrhiza
MOL007108	Isocryptotanshinone	54.98	0.39	Salvia miltiorrhiza
MOL007111	Isodanshenone II	49.92	0.4	Salvia miltiorrhiza
MOL007115	Mairinol	45.04	0.2	Salvia miltiorrhiza
MOL007119	Mitone I	49.68	0.32	Salvia miltiorrhiza
MOL007121	Mitiprolone	36.56	0.37	Salvia miltiorrhiza
MOL007122	Danshenone	38.76	0.25	Salvia miltiorrhiza
MOL007124	Cryptodanshenone ii	39.46	0.23	Salvia miltiorrhiza
MOL007125	Cryptotestosterone	52.49	0.32	Salvia miltiorrhiza
MOL007130	Prolinylglycine	64.37	0.31	Salvia miltiorrhiza
MOL007141	Hydrochloric acid g	45.56	0.61	Salvia miltiorrhiza
MOL007142	Hydrochloric acid j	43.38	0.72	Salvia miltiorrhiza
MOL007145	Salviolone	31.72	0.24	Salvia miltiorrhiza
MOL007150	6-Hydroxy-1-methyl-6-hydroxymethyl-8,9-dihydro-7H-naphthol	75.39	0.46	Salvia miltiorrhiza
MOL007151	Danshenol B	42.67	0.45	Salvia miltiorrhiza
MOL007152	Zidanshen E	42.85	0.45	Salvia miltiorrhiza
MOL007154	Danshenone IIA	49.89	0.4	Salvia miltiorrhiza
MOL007155	6-Hydroxymethyl-1,6-dimethyl-8,9-dihydronaphthalene-7H-naphthalene	65.26	0.45	Salvia miltiorrhiza
MOL007156	Danshenone VI.	45.64	0.3	Salvia miltiorrhiza
MOL007143	Salvilenone I	32.43	0.23	Salvia miltiorrhiza
MOL007120	Mitone II.	71.03	0.44	Salvia miltiorrhiza
MOL007127	1-Methyl-8,9-dihydronaphthalene-7H-naphthalene[5,6-c]benzofuran-6,10,11-trione	34.72	0.37	Salvia miltiorrhiza
MOL007132	3-(3,4-Dihydroxyphenyl)-2-[Z)-3-(3,4-dihydroxyphenyl)propenoyl]oxypropionic acid	109.38	0.35	Salvia miltiorrhiza
MOL007049	4-Methylmitoquinone	34.35	0.23	Salvia miltiorrhiza
MOL000359	β-Sitosterol	36.91	0.75	Rehmannia glutinosa
MOL000449	Ergosterol	43.83	0.76	Rehmannia glutinosa
MOL002211	11,14-Eicosadienoic acid	39.99	0.2	Aconitum carmichaelii
MOL002388	Delphin_qt	57.76	0.28	Aconitum carmichaelii
MOL002392	Deltoin	46.69	0.37	Aconitum carmichaelii
MOL002395	Deoxycornuside lactone	56.3	0.31	Aconitum carmichaelii
MOL002398	Kaempferol	69.56	0.34	Aconitum carmichaelii
MOL002401	New cardosamine B	43.1	0.85	Aconitum carmichaelii
MOL002422	Isothiaretin	50.82	0.73	Aconitum carmichaelii
MOL002434	Carnosifloside Iqt	38.16	0.8	Aconitum carmichaelii
MOL000359	β-Sitosterol	36.91	0.75	Aconitum carmichaelii
MOL001607	ZINC03982454	36.91	0.76	Cynomorium songaricum
MOL003578	Artemisinin	38.69	0.78	Cynomorium songaricum
MOL000358	β-Sitosterol	36.91	0.75	Cynomorium songaricum
MOL004125	Curcumin B_qt	83.36	0.19	Cynomorium songaricum
MOL000449	Ergosterol	43.83	0.76	Cynomorium songaricum

https://doi.org/10.2147/JIR.S506716

Construction of the Active Component Library of BSHXF and the Target Set of OA

The TCMSP database encompassed 1573 targets associated with BSHXF. Leveraging the UniProt database, we retrieved the gene names corresponding to these targets, eliminating any invalid or duplicated entries, culminating in a final set of 189 valid targets. Through comprehensive exploration and integration of major databases, we acquired a total of 2095 OA-related gene targets. By intersecting the target genes derived from the compound (189) with those associated with OA (2095), we identified 99 common target genes. For detailed information, Please refer to Figure 1A.

PPI Network Analysis

The 99 common genes acquired were entered into the STRING database to generate the PPI network. Subsequently, the results were imported into Cytoscape 3.7.2 software to analyze the network's topological parameters. The findings revealed AKT1, TNF, IL-6, and TP53 as the most critical targets, as indicated by the analysis results (Figure 1B).

BSHXF Active Ingredients–Disease Target Network

In constructing the network delineating BSHXF therapeutic targets and their corresponding active ingredients, we employed a bioinformatics approach and imported the data into Cytoscape software for visualization and analysis. As shown in Figure 2, the circular nodes of varied colors in the network denote the active ingredients of five distinct drugs, while the diamond-shaped nodes signify the targets of drug action. The size of these target nodes correlates positively with their importance in the network; thus, larger node sizes denote greater BSHXF therapeutic mechanism. Through component–target topology analysis (Table 2), we found that these active ingredients exhibited the ability to interact with multiple targets in the network, implying their pivotal role in orchestrating the protein interaction network. In particular, the high connectivity of luteolin and tanshinone IIA in the network, suggested their potential as key active components in BSHXF. This finding provides crucial insights for further investigation into the pharmacological mechanisms underlying the action of BSHXF.

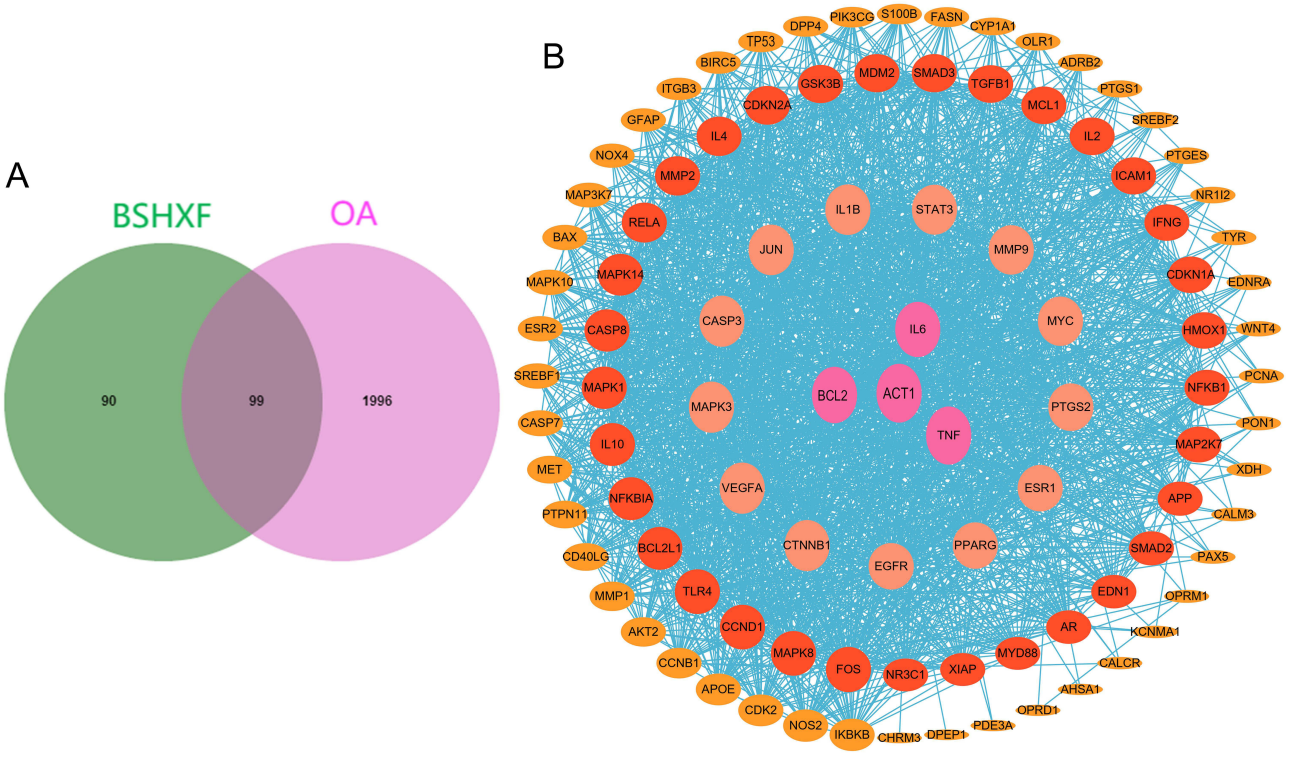

Figure 1 (**A**). Common target of BSHXF and OA. (**B**). In the interaction network of potential targets of BSHX and OA, node size and correlation were positively correlated, and ACT1, TNF, Bcl-2 and IL-6 were the core targets.

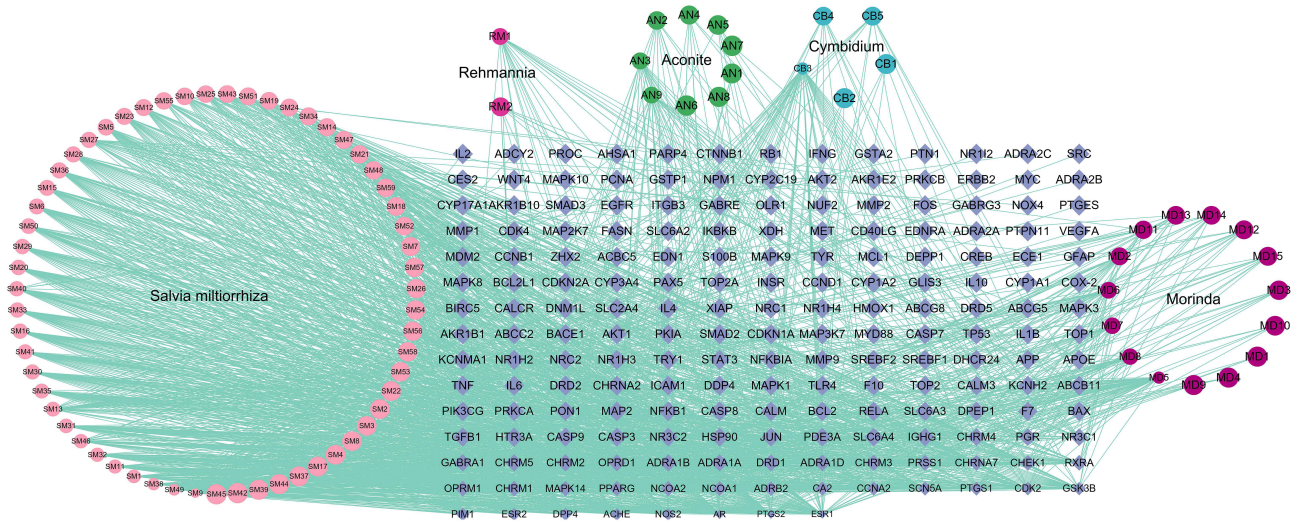

Figure 2 Interaction map of BSHXF ingredients, namely Rehmannia (RM), Salvia miltiorrhiza (SM), Morinda (MD), Cymbidium (CB) and Aconite (AN), and targets.The circle represents the active ingredient of the drug, and the prism represents the target of action.

Biological Function and Signal Pathway Analysis

To elucidate the role of target proteins interacting with BSHXF in gene function and signaling pathways, we conducted GO analysis utilizing the annotation, visualization, and integrated discovery database Metascape (https://metascape.org). The GO analysis encompassed cell components (CCs), molecular functions (MFs), and biological processes (BPs) with a significance level of $p < 0.01$. Additionally, Metascape was employed for KEGG pathway analysis to identify the pathways significantly affected by BSHXF in OA treatment. We selected the top 10 enriched pathways, as shown in Figure 3. The GO analysis revealed that key targets primarily regulate biological processes through DNA-binding transcription factors and cellular oxidative stress response. Changes in cell composition were predominantly observed in the intermembrane space, serine/threonine protein kinase complex, lipid rafts, among others. Molecular function alterations were predominantly associated with cytokine activity, phosphatase activity, RNA polymerase II activity, and specific DNA-binding transcription factors. Furthermore, KEGG pathway analysis demonstrated that key targets were primarily enriched in the IL-17 signaling pathway.

Molecular Docking Analysis of Primary Components

To thoroughly investigate the interaction between two core active ingredients (luteolin and tanshinone IIA) and three key hub genes (Bcl-2, IL-6, and MMP-9), we performed molecular docking experiments. Molecular docking is a computational method used to predict the binding mode and affinity between small molecules (ligands) and proteins (receptors). In this study, we evaluated the binding potential between ligands and receptors using molecular docking technique. Affinity refers to the capacity of the ligand to bind to the receptor, and a lower binding energy (ΔG) signifies a stronger affinity between the ligand and the receptor, facilitating the formation of a stable complex.[42] In addition, we

Table 2 Topological Analysis Results of Main Components of BSHXF

NO	Name	Ingredient	Degree
1	DS9	Luteolin	64
2	DS49	Tanshinone IIA	51
3	BJT5	β-Sitosterol	45
4	XM3	mitiprolone	43
5	DS38	Kaempferol	41

https://doi.org/10.2147/JIR.S506716

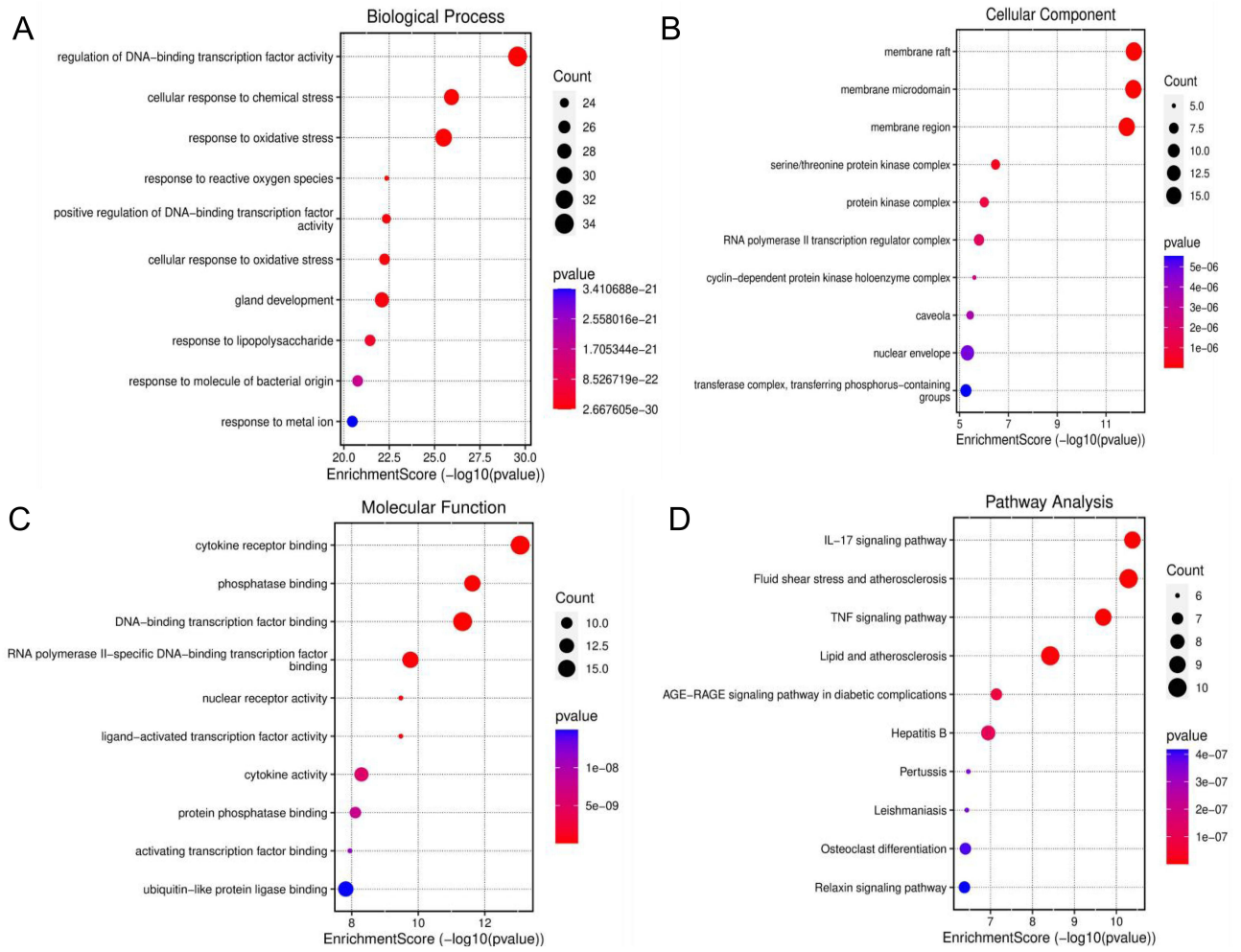

Figure 3 (**A**). Biological processes. (**B**). Cellular components. (**C**). Molecular functions. (**D**). Enriched pathways.

analyzed the potential formation of hydrogen bonds between the ligand and the receptor, which play a key role in stabilizing protein–ligand complexes.[43] The experimental results showed that both luteolin and tanshinone IIA exhibited good molecular docking with Bcl-2, IL-6, and MMP-9. Specifically, detailed binding energy data are presented in Table 3, and the binding sites and hydrogen bond formations are depicted by yellow dashed lines in Figure 4. The results indicated the formation of a more stable complex structure between the active ingredients and the hub genes, thereby furnishing crucial insights into the molecular mechanism of action of BSHXF. In summary, the results of the molecular docking experiments substantiate the hypothesis positing luteolin and tanshinone IIA as key active ingredients in BSHXF. Furthermore, these findings revealed that they may exert pharmacological effects through their interactions with hub genes such as Bcl-2, IL-6, and MMP-9. This finding provides valuable foundational data for subsequent pharmacological investigations and drug design.

Effect of Luteolin and Tanshinone IIA Components of BSHXF on the Activity of Chondrocytes in OA

To assess the effect of various treatments on chondrocyte viability, we employed the CCK-8 assay to determine the effect of different concentrations of IL-1β on chondrocyte viability after 12, 24 and 48 h. We found that 30 ng/mL IL1-β significantly reduced chondrocyte viability (Supplementary Figure 2), whereas ≤10 μM luteolin and ≤20 μM tanshinone IIA exhibited no toxicity on chondrocytes (Supplementary Figures 3A, B). Subsequently, we combined luteolin and tanshinone IIA for intervention in the cells and found that 5 μM luteolin in combination with 10 μM tanshinone IIA effectively inhibited the IL-

Table 3 Binding Energy of Luteolin and Tanshinone IIA Docking with BCL-2, IL-6 and MMP-9

Compound	Binding Energy(Kcal/mol)		
	BCL-2	IL-6	MMP-9
luteolin	−4.35	−3.89	−5.16
Tanshinone IIA	−5.13	−6.17	−5.68

1β-induced decrease in chondrocyte viability without inducing toxicity (Figures 5A and B). We performed Hoechst 33342 staining and flow cytometry to detect chondrocyte apoptosis in the various treatment groups. The results showed that IL-1β significantly increased the rate of chondrocyte apoptosis, indicating that IL-1β could induce apoptosis in chondrocytes. Conversely, co-administration of IL-1β effectively reduced the rate of chondrocyte apoptosis, suggesting that luteolin and tanshinone IIA could protect the chondrocytes against IL-1β-induced apoptosis (Figure 5C, supplementary figures 4). To evaluate the effects of luteolin and tanshinone IIA on IL-1β-induced chondrocyte mortality, we employed the Calcein AM/PI fluorescent staining kit. Calcein AM (calcium xanthophyll) is a cell-activated fluorescent probe that emits a strong green fluorescence following degradation and binding to intracellular calcium ions in living cells, thereby indicating living cells. In contrast, PI is a nucleic acid fluorescent dye that embeds itself in the DNA double helix structure and emits a red fluorescence; however, as it cannot traverse the cell membrane of living cells, it only labels dead cells with impaired cell

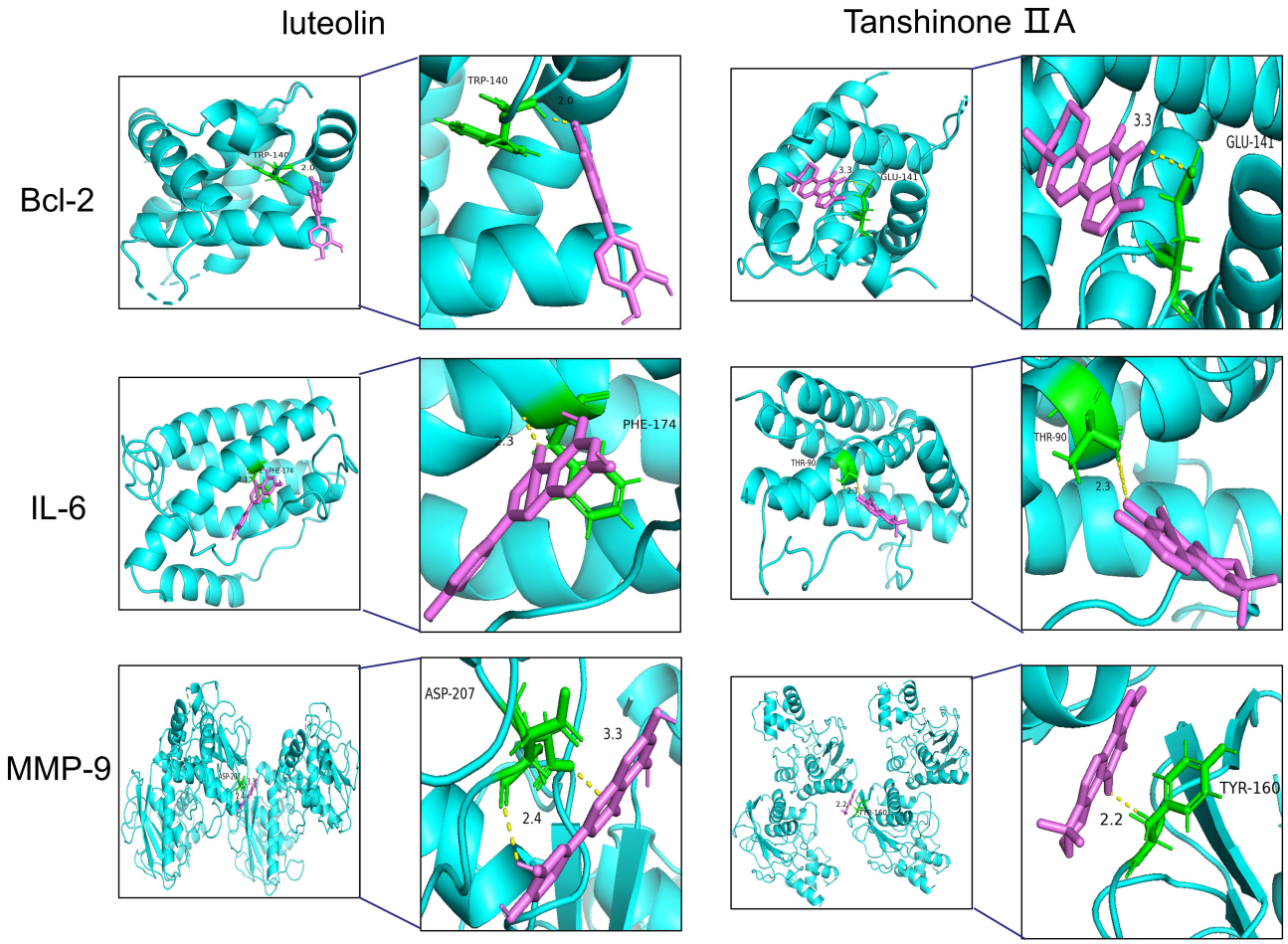

Figure 4 Luteolin and tanshinone IIA were docked with Bcl-2, IL6, and MMP-9, respectively.

https://doi.org/10.2147/JIR.S506716

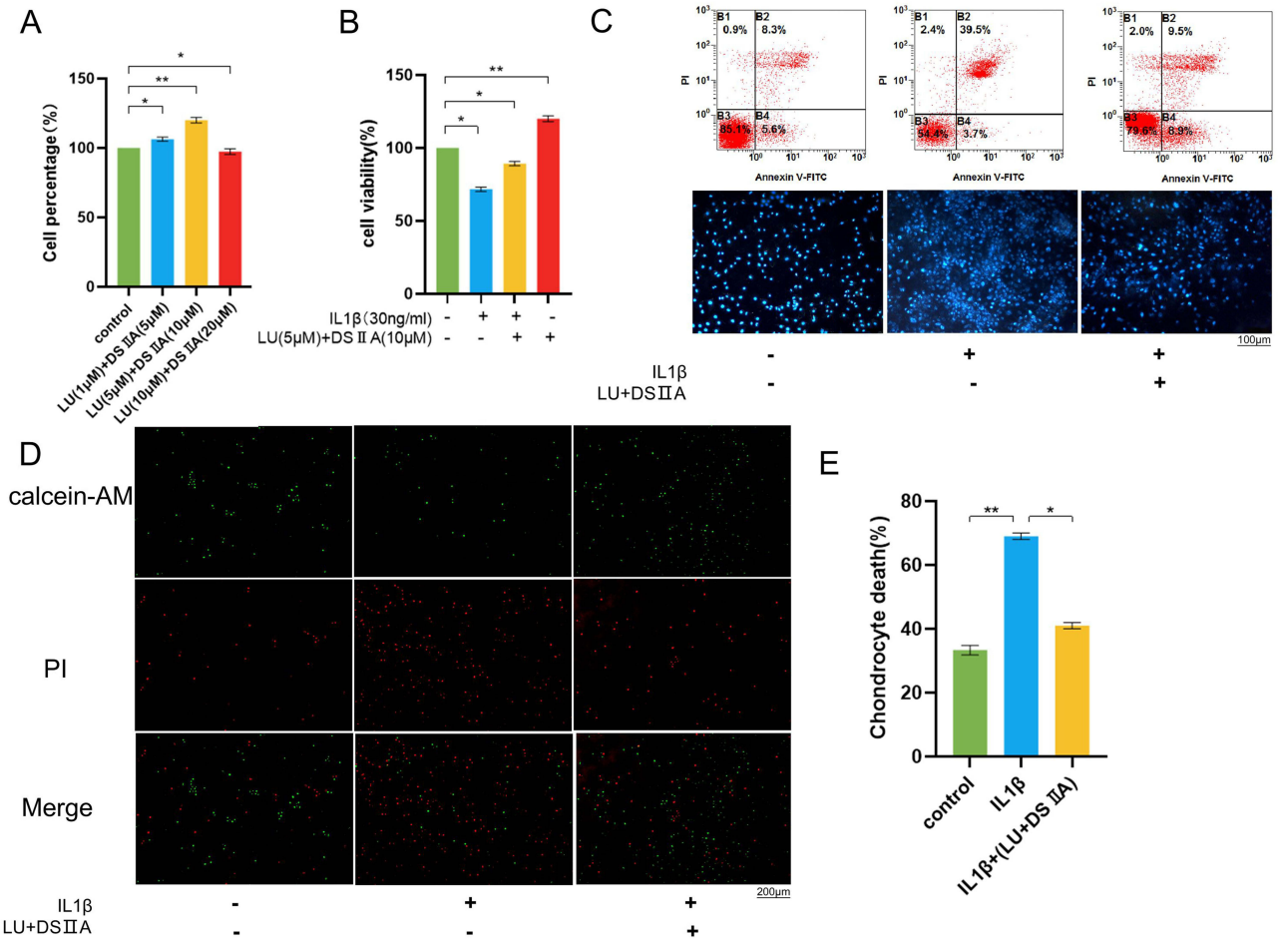

Figure 5 (**A**). Effect of the combined administration of luteolin and tanshinone IIA on cell viability. (**B**). Effect of 5 μM luteolin in combination with 10 μM tanshinone IIA on the activity of inflammatory chondrocytes. (**C**). Hoechst 33342 fluorescence staining (scale, 100 μM), and the results of flow cytometry apoptosis detection. (**D**). Fluorescent staining to evaluate the survival status of chondrocytes (scale, 200 μM). (**E**). Fluorescence staining for quantitative analysis. (n = 3). *$p < 0.05$, ** $p < 0.01$, vs the IL1βgroup.

membrane integrity. In our experiments, we initially treated chondrocytes with 30 ng/mL IL-1β to induce apoptosis. Subsequently, we added 5 μM luteolin and 10 μM tanshinone IIA to examine the effects of these two active ingredients on cell survival. The experimental results were observed via fluorescence microscopy, wherein green fluorescence represented living cells and red fluorescence represented dead cells. The results showed that the mortality rate of chondrocytes was significantly increased following treatment with IL-1β; whereas, the mortality rate of chondrocytes was significantly reduced following treatment with a combination of luteolin and tanshinone IIA (Figures 5D and E). On the basis of these results, we identified the combination of 5 μM luteolin, 10 μM tanshinone IIA, and 30 ng/mL IL-1β as the optimal treatment for subsequent experiments. This finding suggests that luteolin and tanshinone IIA may exert protective effects on chondrocytes by inhibiting the IL-1β-induced apoptotic pathway, providing an experimental basis for further investigation into their potential applications in anti-inflammation and chondroprotection.

Primary Components of BSHXF, Luteolin and Tanshinone IIA, Inhibit IL1-β-Induced Chondrocyte Apoptosis

To thoroughly investigate the molecular mechanism underlying the anti-apoptotic effect of BSHXF on OA chondrocytes, we quantified the expression levels of apoptosis-related proteins, Bcl-2 and caspase-3, utilizing two techniques: western blot and immunofluorescence staining. Initially, we examined the effect of IL-1β on the protein expression of Bcl-2 and caspase-3 through western blot analysis. Bcl-2 is an anti-apoptotic protein and caspase-3 is a key apoptosis execution

protein. The experimental results showed that IL-1β treatment significantly diminished the protein expression level of Bcl-2 while augmenting the protein expression level of caspase-3. This indicated that IL-1β could promote the apoptotic process in chondrocytes (Figures 6A–C). Subsequently, we further validated the western blot results through immunofluorescence staining. Utilizing this technique, we examined the distribution and expression of Bcl-2 and caspase-3 in chondrocytes. The experimental results showed that the protein expression level of Bcl-2 was reduced in IL-1β-treated chondrocytes, consistent with western blot analysis results. Conversely, the protein expression level of caspase-3 was elevated, consistent with the typical changes observed in the apoptosis process. In addition, pretreatment of cells with luteolin and tanshinone IIA led to the restoration of Bcl-2 expression, whereas the expression level of caspase-3 was significantly reduced, suggesting that these two active ingredients significantly inhibited IL-1β-induced apoptosis in chondrocytes (Figures 6D–F). Taken together, these findings suggest that luteolin and tanshinone IIA may exert anti-apoptotic effects by upregulating the expression of anti-apoptotic protein Bcl-2 and/or downregulating the activity of the apoptosis execution protein caspase-3.

Primary Components of BSHXF, Luteolin and Tanshinone IIA, Inhibit the IL1-β-Induced Inflammatory Response and Extracellular Matrix (ECM) Degradation Through the IL-17A Pathway

A series of molecular biology assays were performed to investigate the effects of BSHXF on IL-17A-mediated inflammatory responses and ECM degradation in OA. IL-17A, a pivotal pro-inflammatory cytokine, activates downstream signaling molecules, including ACT1, TRAF6, and NF-κB, which subsequently promote the expression of

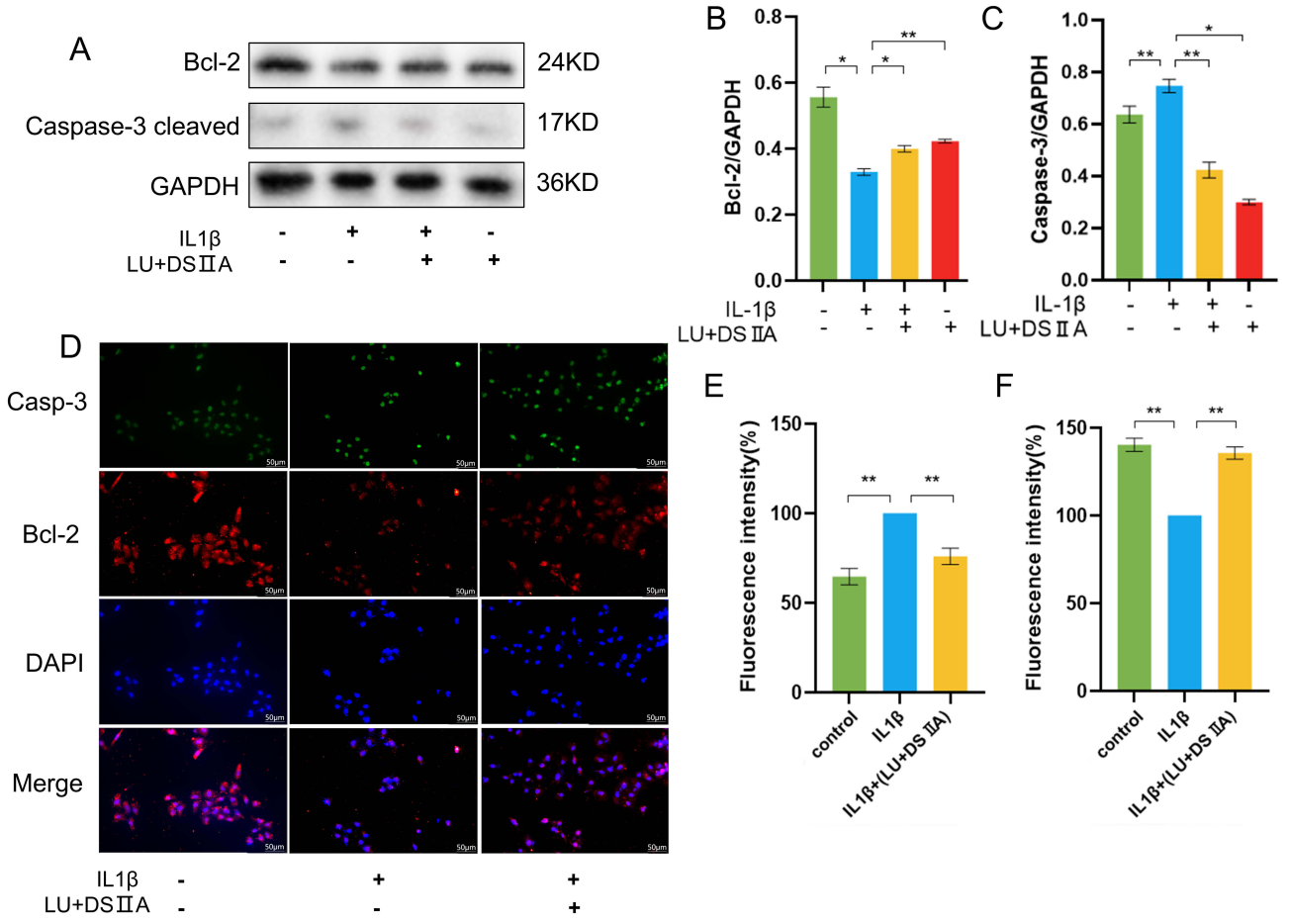

Figure 6 (**A**–**C**). Western blotting and quantitative analysis of Bcl-2 and caspase-3. (**D**). Results of immunofluorescence staining of Bcl-2 and caspase-3. (**E**). Quantitative analysis of caspase-3 via immunofluorescence staining. (**F**). Quantitative analysis of Bcl-2 via immunofluorescence staining. (n = 3). *$p < 0.05$, ** $p < 0.01$, vs the IL1βgroup.

https://doi.org/10.2147/JIR.S506716

inflammatory genes.[44] The inhibition of ACT1, a key activating protein in the IL-17A signaling pathway, has been shown to attenuate the extent of lesions in animal models of OA.[45,46] Initially, we quantified the protein expression levels of IL-17A and its downstream signaling mediator ACT1, through western blot analysis. The results showed that the protein expression of IL-17A and ACT1 was significantly upregulated in IL-1β-treated chondrocytes compared with the normal control group. Moreover, treatment with BSHXF significantly inhibited this upregulation (Figures 7A–C), suggesting that IL-1β stimulation induces the activation of the IL-17A signaling pathway, whereas lignocellulosic acid and tanshinone IIA inhibit its activation. In addition, considering the pivotal role of MMPs in ECM degradation, we further examined the protein expression of MMP-9 and MMP-1. These enzymes degrade key components of the ECM, such as type II collagen and proteoglycans. Western blot analysis revealed that BSHXF significantly reduced the protein expression levels of MMP-9 and MMP-13 induced by IL-1β (Figure 7D–F), suggesting that BSHXF may mitigate ECM degradation by inhibiting the expression of MMPs. To comprehensively assess the effect of BSHXF on the inflammatory response, we also assessed the protein expression of the inflammatory factors IL-6, TNF-α, and the inflammatory mediator COX-2. Western blot results showed that BSHXF treatment significantly reduced IL-1β-induced protein expression of IL-6, TNF-α, and COX-2, effectively inhibiting the inflammatory response (Figure 7G–J). In conclusion, our findings suggest that BSHXF exerts anti-inflammatory and protective effects on OA chondrocytes by inhibiting the IL-17A/ACT1 signaling pathway, decreasing MMP-mediated degradation of ECM, and downregulating the expression of inflammatory factors.

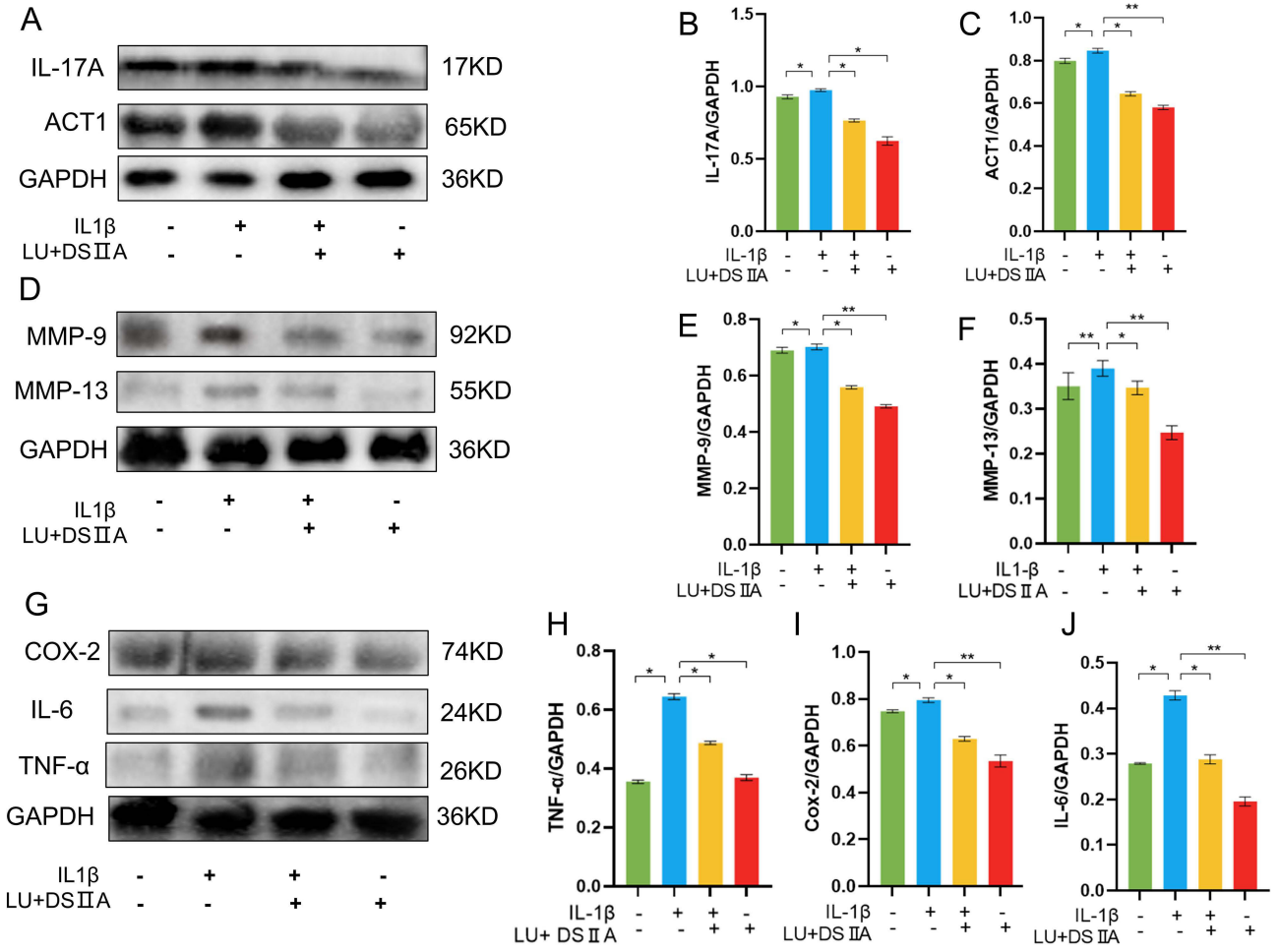

Figure 7 (**A–C**). Western blot imprinting and quantitative analysis of IL-17A and ACT1. (**D–F**). Western blotting and quantitative analysis of MMP-9 and MMP-1. (**G–J**). Western blotting and quantitative analysis of COX-2, IL-6, and TNF-α .(n = 3). *$p < 0.05$, ** $p < 0.01$, vs the IL1βgroup.

BSHXF Attenuates Cartilage Degeneration and Osteophyte Formation

We utilized H&E, SO and TB staining methods to observe and analyze morphological changes in cartilage and bone tissues from different perspectives. HE staining was used to depict the morphology and cellularity of cartilage, SO staining to evaluate the proteoglycan content of cartilage, and TB staining to determine the degree of mineralization in bone and the status of bone resorption. H&E staining showed that cartilage in the sham-operated group exhibited organized morphology, with a columnar arrangement of chondrocytes, abundant cartilage matrix, and a smooth cartilage surface. Conversely, in the surgery group, cartilage displayed severe damage and erosion, reduced chondrocyte count, disordered arrangement, diminished cartilage matrix, and a rough cartilage surface. We observed cartilage repair to some extent in the high-dose treatment group, characterized by an increased number of chondrocytes, well-arranged, adequate cartilage matrix, and smooth cartilage surface. Furthermore, SO staining showed that cartilage in the sham-operated group exhibited a dark blue hue, indicative of heightened levels of cartilage proteoglycans, thereby manifesting good elasticity and resistance to compression. Conversely, cartilage in the surgical group appeared light blue or colorless, indicating diminished cartilage proteoglycan content and poor cartilage elasticity and compression resistance. The cartilage in the high-dose treatment group exhibited a darker blue hue, signifying a restoration of cartilage proteoglycan levels and improvement in cartilage elasticity and compression resistance. Furthermore, in TB staining, bones from the sham-operated group displayed a darker blue tint, reflecting elevated bone mineralization levels and good bone hardness and strength. Conversely, bones from the surgical group exhibited a lighter blue or colorless appearance, indicative of reduced bone mineralization and poor bone hardness and strength. The bones of the surgical group exhibited obvious bony irregularities, indicative of bone hyperplasia and deformity. Conversely, the bones from the high-dose treatment group of BSHXF displayed a darker blue hue, indicating restoration of bone mineralization levels and improvements in bone hardness and strength. To mitigate potential biases, the scoring procedure was performed under blinded conditions, involving five technicians. The methodology considered alterations in cartilage structure, cells, matrix, and surface, with higher scores being associated with more severe cartilage damage. The analysis revealed a significantly elevated OARSI score in the surgery group compared to the sham surgery group. Conversely, the OARSI score was markedly lower in the high-dose treatment group of BSHXF compared to the surgery group, indicating that BSHXF administration at a high dose mitigated cartilage damage (Figure 8B). In conclusion, these results indicate that high-dose administration of BSHXF significantly increased cartilage thickness, enhanced cartilage morphology and function, and reduced the OARSI score in OA rats. Additionally, it ameliorated impaired bone mineralization and osteochondral conditions, thus exerting a protective effect on both cartilage and bone in OA rats.

BSHXF Inhibits Synovial Inflammatory Factors in a Surgically Induced OA Model

We quantified the levels of inflammatory cytokines IL-1β, IL-6, and TNF-α in the synovial fluid from rats at weeks 4, 8, and 12 through ELISA. Inflammatory factors IL-1β, IL-6, and TNF-α are pivotal cytokines capable of initiating an inflammatory response, playing a crucial role in the pathogenesis of OA by stimulating chondrocytes to release MMPs and oxidative stress substances, thereby contributing to cartilage degradation and damage. Our findings revealed significantly elevated levels of IL-1β, IL-6, and TNF-α in both bone tissue and articular fluid samples from the surgery group compared to those from the sham surgery group. This suggests that surgical intervention can induce inflammation in OA rats. Furthermore, we observed markedly reduced levels of IL-1β, IL-6, and TNF-α in the osteoarticular fluid samples obtained from the BSHXF treatment group compared to those derived from the operation group. These results indicate that BSHXF exhibits anti-inflammatory properties in OA rats (Figure 8C).

BSHXF Improves Subchondral Bone Resorption

To investigate the impact of the BSHXF on bone morphology in rats with OA, we employed micro-CT for three-dimensional bone reconstruction and quantified several morphological parameters: BV/TV, Tb.Th, Tb.N, and trabecular spacing (Tb.Sp). These parameters are indicative of bone density, strength, integrity, and their association with osteoporosis and bone remodeling. Our investigation revealed that surgical injury induced significant osteophyte formation and increased bone resorption, indicating that OA progression led to both proliferation and destruction of

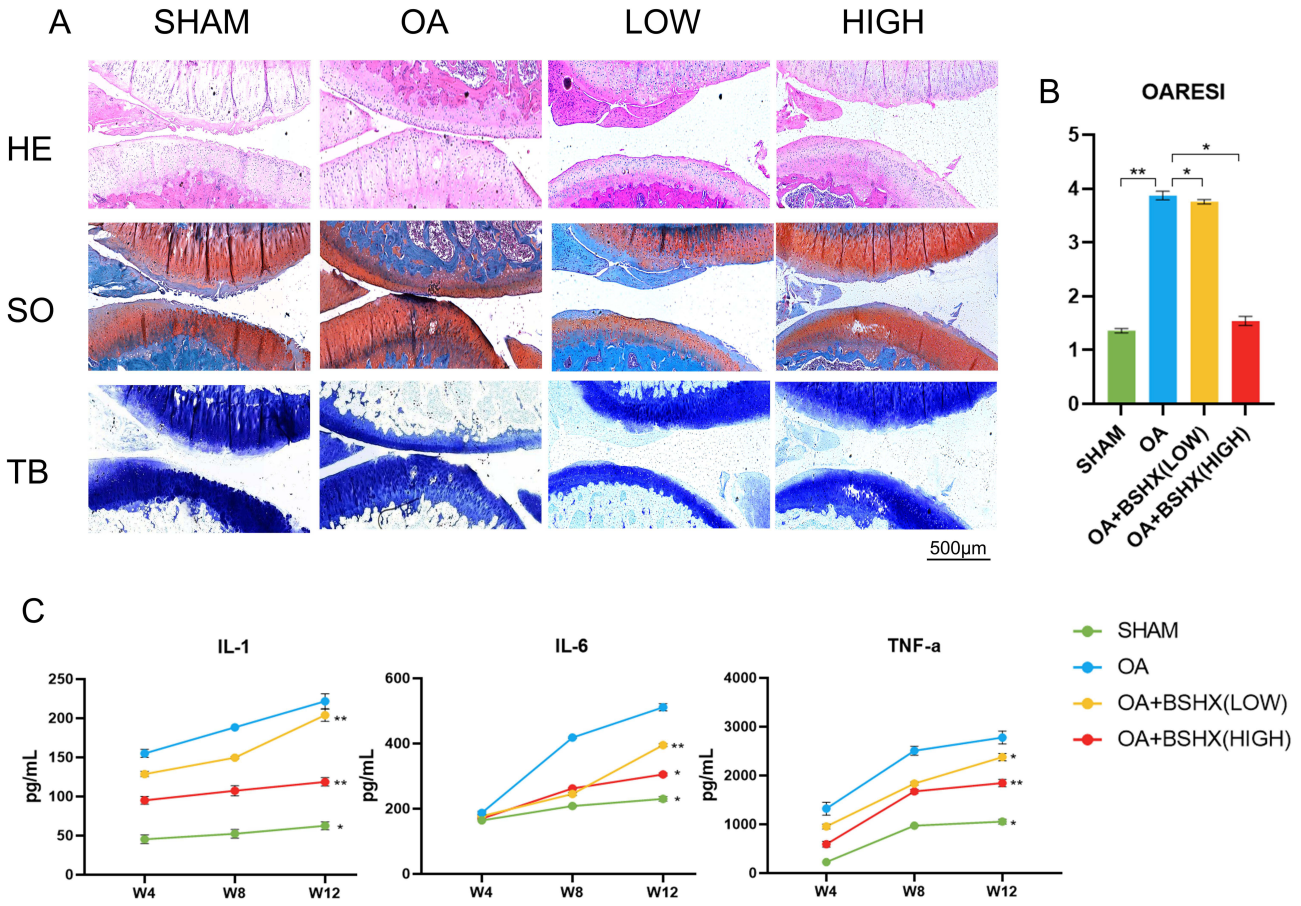

Figure 8 (**A**). Representative HE, SO, and TB staining (scale, 500 μM) of cartilage from various experimental groups (sham operation group, OA group, OA + BSHX (LOW) group, and OA + BSHX (HIGH) group). (**B**). Cartilage OARSI scores for four groups. (**C**). The expression levels of IL-6, TNF-a, and IL-1 in rat articular fluid were assessed at 4, 8, and 12 weeks . (n = 5).*$p < 0.05$, ** $p < 0.01$, vs the OA group.

bone tissue. The administration of the BSHXF significantly increased BV/TV, Tb.Th, and Tb.N, while concomitantly decreasing Tb.Sp in OA rats, suggesting an improvement in bone density, strength, and integrity attributable to this treatment approach (Figure 9A). To quantitatively assess extent of changes in bone morphology, we employed ANOVA followed by Tukey's test for comparing the various groups. The results revealed a significant reduction in BV/TV, Tb. Th., and Tb.N in the surgery group compared to the sham operation group; however, Tb.Sp exhibited a significant increase. Conversely, upon treatment with BSHXF, BV/TV, Tb.Th, and Tb.N were significantly elevated, while Tb.Sp was notably decreased (Figure 9B). In conclusion, these results indicate that BSHXF can effectively inhibit morphological changes occurring within bones of OA rats, thereby playing a protective role.

Discussion

Chondrocyte apoptosis and ECM degradation are common pathological features of OA. The ECM predominantly comprises type 2 collagen, susceptible to degradation by matrix-degrading enzymes such as MMPs.[42] In OA, inflammatory factors, such as TNF-α, IL-6, and IL-1β, are prevalent, ECM degradation and the accumulation of these inflammatory substances can exacerbate the degradation of the ECM while promoting chondrocyte apoptosis.[43] Conversely, the products of chondrocyte apoptosis and matrix decomposition stimulate the production of inflammatory substances, further exacerbating OA.[43,47] BSHXF has been found to inhibit MMP13 signaling in chondrocytes, inhibiting ECM degradation and promoting tissue repair.[48]

Network pharmacological studies have revealed the key targets of BSHXF in the treatment of OA, including TNF-α, Bcl-2, and IL-6. TNF-α, a potent pro-inflammatory factor binds to two types of receptors, namely TNFR1 and TNFR2,

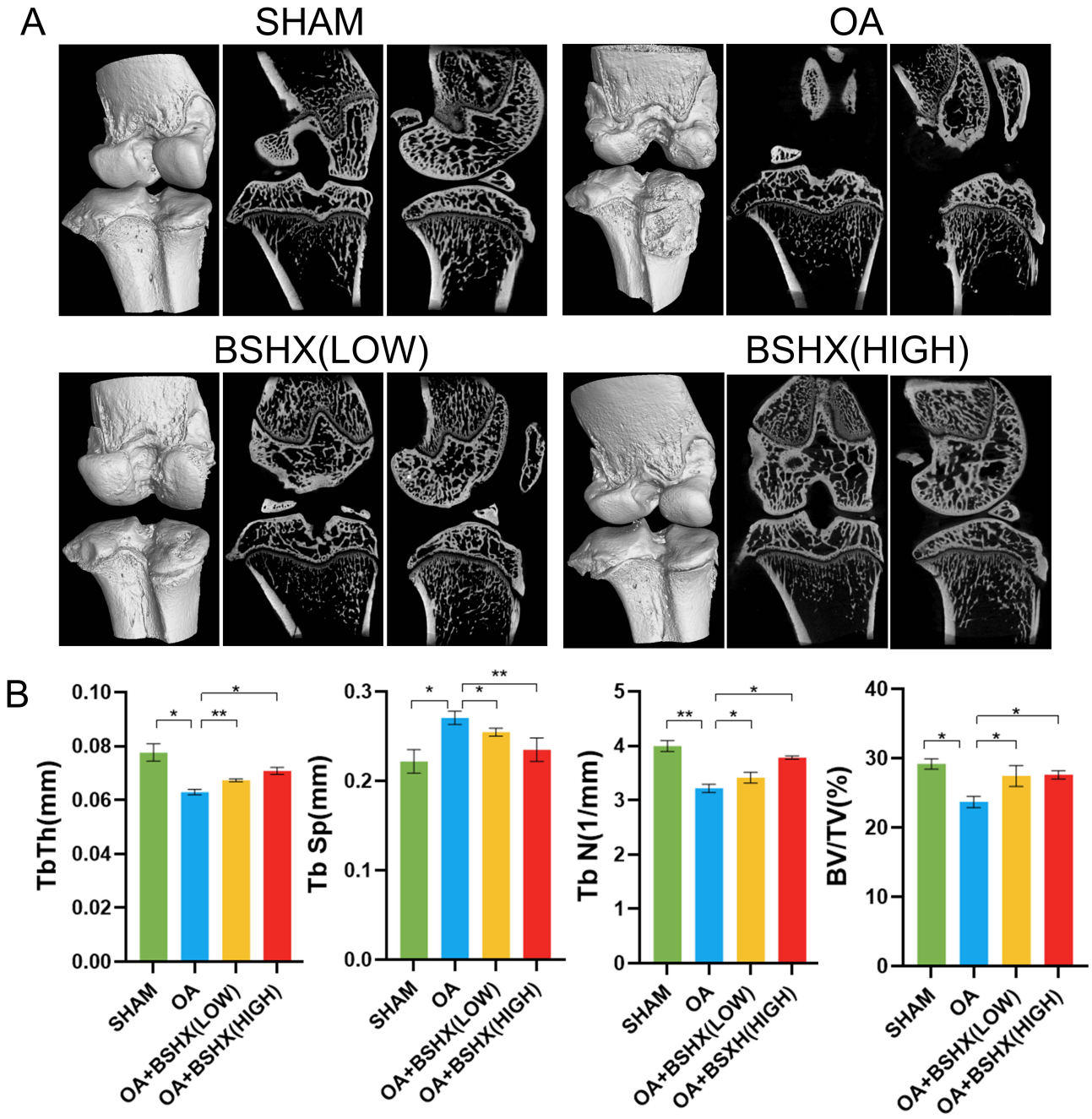

Figure 9 (**A**). The knee joint was reconstructed in three dimensions, with the sagittal and coronal planes displayed. (**B**). Quantitative analysis of Tb.Th, Tb.Sp, TB-N, and BV/TV. (n = 3).*$p < 0.05$, **$p < 0.01$, vs the OA group.

expressed on the surface of chondrocytes and synoviocytes.[49] This binding triggers the downstream activation of the NF-κB signaling pathway. Moreover, IL-6 exerts its influence on chondrocytes by inhibiting ECM degradation and fostering tissue repair.[50] IL-6, also recognized as a typical inflammatory factor, binds to the membrane-bound IL-6-specific receptor IL-6Rα, thereby activating classical signaling pathways such as the p38 and Signal Transducers and Activators of Transcription (STAT) pathways. The combined effect of these factors leads to the upregulation of inflammatory mediators and matrix-degrading enzymes synthesis while concurrently inhibiting the synthesis of type II collagen.[50,51] Bcl-2, a key anti-apoptotic protein, sustains cell viability by counteracting pro-apoptotic signals.[52] During the pathological progression of OA, the expression level of Bcl-2 significantly influences the apoptotic susceptibility of chondrocytes. The downregulation of Bcl-2 expression is closely associated with the development of OA, as it attenuates

https://doi.org/10.2147/JIR.S506716

the protective effect on chondrocytes, rendering these cells more prone to apoptosis.[53] As the number of apoptotic cells increases, there is a corresponding decline in the number of functional chondrocytes, directly impacting the synthesis and maintenance of ECM proteins.[54] Therefore, by regulating the expression or biological functions of TNF-α, Bcl-2, and IL-6, novel therapeutic avenues for OA may be explored, potentially delaying or halting the pathological progression of OA. Our findings suggest that BSHXF effectively inhibits chondrocyte apoptosis, downregulates the expression of inflammatory mediators, and inhibits ECM degradation.

The IL-17 cytokine family comprises six structurally related cytokines, namely IL-17A to IL-17F. IL-17A (commonly referred to as IL-17) is the quintessential member of its family, garnering considerable attention for its pro-inflammatory role in autoimmune diseases.[44] Moreover, IL-17 plays important environmental and tissue-dependent roles in the maintenance of health in response to injury, physiological stress, and infection.[44,46] Consequently, the IL-17 pathway has emerged as a prominent drug target in many autoimmune and chronic inflammatory diseases. Targeting the IL-17A receptor has demonstrated notable efficacy in the treatment of some of these diseases.[45] A study reported that intra-articular injection of IL-17-neutralizing antibodies leads to reduced joint degeneration and decreased expression of the aging marker Cdkn1a.[46] This study revealed that BSHXF significantly inhibits the activation of the IL-17A signaling pathway. The underlying mechanism involves delaying chondrocyte apoptosis through downregulating the expression of the key signaling molecule ACT1, while effectively suppressing the matrix metalloproteinases (MMPs)-mediated extracellular matrix degradation process.

Luteolin, a naturally occurring flavonoid compound, has garnered significant attention for its remarkable biological activities. In the biomedical field, luteolin demonstrates both anti-inflammatory and anti-catabolic effects, offering multifaceted benefits for health maintenance.[55] Recent scientific advancements have revealed the potential of luteolin in reversing the degradation of collagen type II induced by IL-1β. In vitro experimental data showed that luteolin significantly inhibits IL-1β-induced phosphorylation of NF-κB, suggesting its potential inhibitory role in inflammatory responses in OA. In addition, animal experiments have further corroborated the positive effects of luteolin in reducing cartilage destruction and enhancing type II collagen expression in a rat model of OA.[56] In addition, the inhibitory effect of luteolin on hydrogen peroxide (H_2O_2)-induced cell death, apoptosis, oxidative stress, programmed necrosis, and inflammatory mediator production in primary mouse chondrocytes is closely associated with its activation of the AMP-activated protein kinase (AMPK) and nuclear factor E2-associated factor 2 (Nrf2) signaling pathways.[57] The experimental results of this study align with these findings and provide further substantiation for the potential application of luteolin in the treatment of OA.

Tanshinone IIA, one of the active constituents in Salvia miltiorrhiza, has demonstrated various pharmacological effects, including anti-inflammatory, antioxidant, and anti-apoptotic properties.[58] In recent years, several studies have revealed the potential efficacy of tanshinone IIA in OA treatment. Specifically, tanshinone IIA has been shown to significantly reduce the levels of inflammatory factors, including IL-1β, TNF-α, and Inducible nitric oxide synthase,[59] in the articular cartilage of OA model rats, thereby effectively attenuating the inflammatory response and chondrocyte damage, which aligns with our experimental findings. Moreover, a study conducted by Xu et al[60] further indicated that tanshinone IIA alleviates chondrocyte apoptosis by inhibiting ferroptosis and inhibits the degradation of the ECM. In addition, tanshinone IIA has been observed to enhance the expression of IL-1β-inhibited Nuclear Enrichment Abundant Transcript 1(NEAT1), a phenomenon that may promote cartilage regeneration in an inflammatory milieu by modulating the transcription of genes associated with chondrocyte phenotype.[61]

Previous studies have revealed the potential protective effect of BSHXF against OA. The mechanism involves the down-regulation of MMP13 expression through the TGF-β signaling pathway, which inhibits chondrocyte degradation. Additionally, BSHXF inhibits the expression of apoptosis-related proteins CASP3, CASP8, and CASP9, reducing chondrocyte apoptosis and slowing down the pathological process of OA.[29,30] Although we experimentally verified the mechanism of luteolin and tanshinone in BSHXF regulating OA through IL-17A, the multi-target mechanism has not been fully resolved, and its effective dose in OA patients still needs to be explored.Future studies should build on this foundation and conduct more extensive clinical studies and mechanism investigations to provide a solid scientific foundation for the application of the kidney tonifying and blood activating formula in OA treatment and promote its wide application in clinical practice.

Conclusion

In this study, we comprehensively analyzed and predicted the molecular mechanism through which BSHXF treats OA employing a network pharmacology approach, successfully identifying 99 potential targets associated with the pathological progression of OA. Subsequent bioinformatics analyses identified core targets, such as TNF-α and Bcl-2, and principal components, such as tanshinone IIA and luteolin. KEGG analysis revealed the key signaling pathways influenced by BSHXF in OA. In addition, molecular docking techniques were employed to validate the affinity between key targets and the principal components of BSHXF. In vitro experiments were conducted to assess the protective effects of BSHXF on chondrocytes, while in vivo experiments were conducted to evaluate its ameliorative effects on joint inflammation and cartilage damage using an animal model of OA. This study provides a novel strategy and theoretical underpinning for the treatment of OA with TCM. This study has several limitations. The reliance on rodent models may not fully replicate the heterogeneous nature of human diseases. Variations in serum component analysis preprocessing could affect result reproducibility. Additionally, the retrospective design introduces potential data integrity issues, as non-standardized dosage documentation and confounding factors (including patients' concomitant medications and lifestyle variations) might compromise therapeutic efficacy evaluation. Future research should prioritize multicenter randomized controlled trials to optimize dosing regimens, employ multi-omics technologies (such as spatial transcriptomics coupled with CRISPR validation) to elucidate molecular mechanisms, and establish cross-regional clinical databases to enhance evidence generalizability.

Ethical Approval

The study involved human data from the public database GeneCard, DisGeNET. GeneCard and DisGeNET belong to public databases, and users can download relevant data for free to conduct research and publish relevant articles. All animal experiments were conducted in accordance with the National Institutes of Health (NIH) Guidelines for the Care and Use of Laboratory Animals and have been approved by the Ethics Committee of Xi'an Jiaotong University (Approval No. 2024-1590).

Acknowledgments

This work was supported by the Shaanxi Province Key Research and Development Plan (2020SF-099),Shaanxi Province Innovation Capability Support Plan (2021TD-59),Shaanxi Province Key Research and Development General Project-Social Development Field (2023-YBSF-488) and Xi'an Municipal Health Commission Cultivation Project (2023ms15).

Disclosure

The authors declare that there are no conflicts of interest.

References

1. Tang S, Zhang C, Oo WM, et al. Osteoarthritis. *Nat Rev Dis Primers*. 2025;11:article10.
2. Abramoff B, Caldera FE. Osteoarthritis: pathology, diagnosis, and treatment options. *Med Clin North Am*. 2020;104(2):293–311. doi:10.1016/j.mcna.2019.10.007
3. Nedunchezhiyan U, Varughese I, Sun AR, et al. Obesity, inflammation, and immune system in osteoarthritis. *Front Immunol*. 2022;13:article907750. doi:10.3389/fimmu.2022.907750
4. Sánchez-Romero EA, Pecos-Martín D, Calvo-Lobo C, et al. Clinical features and myofascial pain syndrome in older adults with knee osteoarthritis by sex and age distribution: a cross-sectional study. *Knee*. 2019;26(1):article165–173. doi:10.1016/j.knee.2018.09.011
5. Yunus MHM, Nordin A, Kamal H. Pathophysiological perspective of osteoarthritis. *Medicina*. 2020;56(11):614. doi:10.3390/medicina56110614
6. Meléndez-Oliva E, Martínez-Pozas O, Sinatti P, et al. Relationship between the gut microbiome, tryptophan-derived metabolites, and osteoarthritis-related pain: a systematic review with meta-analysis. *Nutrients*. 2025;17(2):article264. doi:10.3390/nu17020264
7. Georgiev T, Angelov AK. Modifiable risk factors in knee osteoarthritis: treatment implications. *Rheumatol Inter*. 2019;39(7):1145–1157. doi:10.1007/s00296-019-04290-z
8. Zhang BH, Zhang Y, Chen C, et al. Pioglitazone inhibits advanced glycation end product-induced matrix metalloproteinases and apoptosis by suppressing the activation of MAPK and NF-κB. *Apoptosis Int J Program Cell Death*. 2016;21(10):1082–1093. doi:10.1007/s10495-016-1280-z
9. Monti D, Ostan R, Borelli V, et al. "Inflammaging and human longevity in the omics era. *Mechan Age Develop*. 2017;165(Pt B):129–138. doi:10.1016/j.mad.2016.12.008
10. Hu J, Wang Z, Pan Y, et al. "MiR-26a and miR-26b mediate osteoarthritis progression by targeting FUT4 via NF-κB signaling pathway. *Int J Biochem Cell Biol*. 2018;94:79–88. doi:10.1016/j.biocel.2017.12.003

11. Sánchez-Romero EA, Battaglino A, Campanella W, et al. Impact on blood tests of lower limb joint replacement for the treatment of osteoarthritis: hip and knee. *Top Geriatric Rehabil*. 2021;37(4):article227–229. doi:10.1097/TGR.0000000000000337
12. Jaswal AP, Bandyopadhyay A. Re-examining osteoarthritis therapy from a developmental biologist's perspective. *Biochem Pharmacol*. 2019;165:17–23. doi:10.1016/j.bcp.2019.03.020
13. Pettenuzzo S, Arduino A, Belluzzi E, et al. Biomechanics of chondrocytes and chondrons in healthy conditions and osteoarthritis: a review of the mechanical characterisations at the microscale. *Biomedicines*. 2023;11(7):article1942. doi:10.3390/biomedicines11071942
14. Battistelli M, Favero M, Burini D, et al. Morphological and ultrastructural analysis of normal, injured and osteoarthritic human knee menisci. *Eur J Histochem*. 2019;63(1):article2998. doi:10.4081/ejh.2019.2998
15. Favero M, El-Hadi H, Belluzzi E, et al. Infrapatellar fat pad features in osteoarthritis: a histopathological and molecular study. *Rheumatology*. 2017;56(10):article1784–1793. doi:10.1093/rheumatology/kex287
16. Vincent TL, Alliston T, Kapoor M, et al. Osteoarthritis pathophysiology: therapeutic target discovery may require a multifaceted approach. *Clin Geriatric Med*. 2022;38(2):193–219. doi:10.1016/j.cger.2021.11.015
17. Ahmed GO, ELSweify K, Ahmed AF. Usability of the AAOS appropriate use criteria (AUC) for the surgical management of knee osteoarthritis in clinical practice. *Knee Surg Sports Traumatol Arthrosc*. 2020;28(7):2077–2081. doi:10.1007/s00167-020-05908-7
18. Millerand M, Berenbaum F, Jacques C. Danger signals and inflammaging in osteoarthritis. *Clin Experi Rheumatol*. 2019;120(5):48–56.
19. Kraus VB, Karsdal MA. Clinical monitoring in osteoarthritis: biomarkers. *Osteoarthritis Cartilage*. 2022;30(9):1159–1173. doi:10.1016/j.joca.2021.04.019
20. Ceballos-Laita L, Estébanez-de-Miguel E, Martín-Nieto G, et al. Effects of non-pharmacological conservative treatment on pain, range of motion and physical function in patients with mild to moderate hip osteoarthritis: a systematic review. *Complement Ther Med*. 2019;42:214–222. doi:10.1016/j.ctim.2018.11.021
21. Sánchez-Romero EA, Fernández-Carnero J, Calvo-Lobo C, et al. Is a combination of exercise and dry needling effective for knee oa?. *Pain Med*. 2020;21(2):article349–363. doi:10.1093/pm/pnz036
22. Hartnett DA, Milner JD, DeFroda SF. Osteoarthritis in the upper extremity. *Ame J Med*. 2023;136(5):415–421. doi:10.1016/j.amjmed.2023.01.025
23. Sherman SL, Thyssen E, Nuelle CW. Osteochondral autologous transplantation. *Clin Sports Med*. 2017;36(3):489–500. doi:10.1016/j.csm.2017.02.006
24. Frehner F, Benthien JP. Microfracture: state of the art in cartilage surgery?. *Cartilage*. 2018;9(4):339–345. doi:10.1177/1947603517700956
25. Oo WM, Yu SP, Daniel MS, et al. Disease-modifying drugs in osteoarthritis: current understanding and future therapeutics. *Exp Opin Emerg Drugs*. 2018;23(4):331–347. doi:10.1080/14728214.2018.1547706
26. Zhang B, Xu H, Wang J, et al. A narrative review of non-operative treatment, especially traditional Chinese medicine therapy, for lumbar intervertebral disc herniation. *Biosci Trends*. 2017;11(4):406–417. doi:10.5582/bst.2017.01199
27. Chen G, Ye X, Guan Y, et al. Effects of Bushen Huoxue method for knee osteoarthritis: a protocol for systematic review and meta-analysis. *Medicine*. 2020;99(24):articlee20659. doi:10.1097/MD.0000000000020659
28. Luo D, Hou Y, Zhan J, et al. BushenhuoXue formula provides neuroprotection against spinal cord injury by inhibiting oxidative stress by activating the Nrf2 signaling pathway. *Drug Des Devel Ther*. 2024;18:article4779–4797. doi:10.2147/DDDT.S487307
29. Wang PE, Zhang L, Ying J, et al. Bushenhuoxue formula attenuates cartilage degeneration in an osteoarthritic mouse model through TGF-β/MMP13 signaling. *J Transl Med*. 2018;16(1):72. doi:10.1186/s12967-018-1437-3
30. Xu HH, Li SM, Xu R, et al. Predication of the underlying mechanism of Bushenhuoxue formula acting on knee osteoarthritis via network pharmacology-based analyses combined with experimental validation. *J Ethnopharmacol*. 2020;263:article113217. doi:10.1016/j.jep.2020.113217
31. Xiong W, Zhao J, Ma X, et al. Mechanisms and molecular targets of Bushenhuoxue formula forOsteoarthritis. *ACS omega*. 2022;7(5):4703–4713. doi:10.1021/acsomega.1c07270
32. Zhan JW, Li KM, Zhu LG, et al. Efficacy and safety of bushen huoxue formula in patients with discogenic low-back pain: a double-blind, randomized, placebo-controlled trial. *Chin J Integr Med*. 2022;28(11):article963–970. doi:10.1007/s11655-022-3505-4
33. Nogales C, Mamdouh ZM, List M, et al. Network pharmacology: curing causal mechanisms instead of treating symptoms. *Trends Pharmacol Sci*. 2021;43(2):136–50.
34. Pinzi L, Rastelli G. Molecular docking: shifting paradigms in drug discovery. *Inter J Molecular Sci*. 2019;20(18):4331. doi:10.3390/ijms20184331
35. Xu Z, Wang C, Luan Z, et al. "Exploring the potential targets of the Abrus cantoniensis Hance in the treatment of hepatitis E based on network pharmacology. *Front Veterin Sci*. 2023;10:article1155677. doi:10.3389/fvets.2023.1155677
36. Mok SR, Mohan S, Grewal N, et al. "A genetic database can be utilized to identify potential biomarkers for biphenotypic hepatocellular carcinoma-cholangiocarcinoma. *J Gastrointest Oncol*. 2016;7(4):570–579. doi:10.21037/jgo.2016.04.01
37. Piñero J, Queralt-Rosinach N, Bravo À, et al. DisGeNET: a discovery platform for the dynamical exploration of human diseases and their genes. *J Biolog Databases Cur*. 2015;2015:articlebav028. doi:10.1093/database/bav028
38. Franz M, Lopes CT, Huck G, et al. Cytoscape.js: a graph theory library for visualisation and analysis. *Bioinformatics*. 2016;32(2):309–311. doi:10.1093/bioinformatics/btv557
39. Batool K, Niazi MA. Towards a methodology for validation of centrality measures in complex networks. *PloS One*. 2014;9(4):articlee90283. doi:10.1371/journal.pone.0090283
40. Sato N, Uematsu M, Fujimoto K, et al. ggkegg: analysis and visualization of KEGG data utilizing the grammar of graphics. *Bioinformatics*. 2023;39(10):articlebtad622. doi:10.1093/bioinformatics/btad622
41. Liew JW, King LK, Mahmoudian A, et al. "A scoping review of how early-stage knee osteoarthritis has been defined. *Osteoarthritis Cartilage*. 2023;31(9):1234–1241. doi:10.1016/j.joca.2023.04.015
42. Baumann HM, Dybeck E, McClendon CL, et al. Broadening the scope of binding free energy calculations using a separated topologies approach. *J Chem Theory Comput*. 2023;19(15):5058–5076. doi:10.1021/acs.jctc.3c00282
43. Renati P, Madl P. What is the 'hydrogen bond?' A QFT-QED perspective. *Inter J Molecular Sci*. 2024;25(7):3846. doi:10.3390/ijms25073846
44. McGeachy MJ, Cua DJ, Gaffen SL. The IL-17 family of cytokines in health and disease. *Immunity*. 2019;50(4):892–906. doi:10.1016/j.immuni.2019.03.021
45. Mills KHG. "IL-17 and IL-17-producing cells in protection versus pathology. *Nat Rev Immunol*. 2023;23(1):38–54. doi:10.1038/s41577-022-00746-9

46. Faust HJ, Zhang H, Han J, et al. IL-17 and immunologically induced senescence regulate response to injury in osteoarthritis. *J Clin Invest*. 2020;130(10):5493–5507. doi:10.1172/JCI134091
47. Hwang HS, Kim HA. Chondrocyte apoptosis in the pathogenesis of osteoarthritis. *Inter J Molecular Sci*. 2015;16(11):26035–26054. doi:10.3390/ijms161125943
48. Gao S, Wang C, Qi L, et al. Bushenhuoxue formula inhibits IL-1β-induced apoptosis and extracellular matrix degradation in the nucleus pulposus cells and improves intervertebral disc degeneration in rats. *J Inflamm Res*. 2024;17:article121–136. doi:10.2147/JIR.S431609
49. Ansari MY, Ahmad N, Haqqi TM. Oxidative stress and inflammation in osteoarthritis pathogenesis: role of polyphenols. *Biomed Pharmacother*. 2020;129:article110452. doi:10.1016/j.biopha.2020.110452
50. Wojdasiewicz P, Poniatowski ŁA, Szukiewicz D. The role of inflammatory and anti-inflammatory cytokines in the pathogenesis of osteoarthritis. *Med Inflamm*. 2014;2014:1–19. doi:10.1155/2014/561459
51. Aigner T, Kim HA, Roach HI. Apoptosis in osteoarthritis. *Rheumatic Dis Clin*. 2024;30(3):639–653. doi:10.1016/j.rdc.2004.04.002
52. Ke D, Xu H, Han J, et al. Curcumin suppresses RANKL-induced osteoclast precursor autophagy in osteoclastogenesis by inhibiting RANK signaling and downstream JNK-BCL2-Beclin1 pathway. *Biomed J*. 2024;47(1):article100605. doi:10.1016/j.bj.2023.100605
53. Pan X, Li X, Zhang L, et al. Umbilical cord mesenchymal stem cells relieve osteoarthritis in rats through immunoregulation and inhibition of chondrocyte apoptosis. *Sci Rep*. 2023;13(1):14975. doi:10.1038/s41598-023-42349-x
54. Li W, Tao C, Mao M, et al. The Nrf2/HMGB1/NF-κB axis modulates chondrocyte apoptosis and extracellular matrix degradation in osteoarthritis. *Acta Biochim Biophys Sin*. 2023;55(5):818–830. doi:10.3724/abbs.2023078
55. Tesio AY, Robledo SN. Analytical determinations of luteolin. *BioFactors*. 2021;47(2):141–164. doi:10.1002/biof.1720
56. Fei J, Liang B, Jiang C, et al. Luteolin inhibits IL-1β-induced inflammation in rat chondrocytes and attenuates osteoarthritis progression in a rat model. *Biomed Pharmacother*. 2019;109(109):1586–1592. doi:10.1016/j.biopha.2018.09.161
57. Zhou Z, Zhang L, Liu Y, et al. Luteolin Protects Chondrocytes from H2O2-induced oxidative injury and attenuates osteoarthritis progression by activating AMPK-Nrf2 signaling. *Oxid Med Cell Longev*. 2022;2022:article5635797. doi:10.1155/2022/5635797
58. Guo R, Li L, Su J, et al. Pharmacological activity and mechanism of tanshinone IIA in related diseases. *Drug Des Devel Ther*. 2020;14:4735–4748. doi:10.2147/DDDT.S266911
59. Wang X, Fan J, Ding X, et al. Tanshinone I inhibits IL-1β-induced apoptosis, inflammation and extracellular matrix degradation in chondrocytes CHON-001 cells and attenuates murine osteoarthritis. *Drug Design Develop Therap*. 2019;13:3559–3568. doi:10.2147/DDDT.S216596
60. Xu J, Zhi X, Zhang Y, et al. "Tanshinone IIA alleviates chondrocyte apoptosis and extracellular matrix degeneration by inhibiting ferroptosis. *Open Life Sci*. 2023;18(1):article20220666. doi:10.1515/biol-2022-0666
61. Sun J, Chen W, Zhou Z, et al. Tanshinone IIA facilitates efficient cartilage regeneration under inflammatory factors caused stress via upregulating LncRNA NEAT1_2. *Biomedicines*. 2023;11(12):3291. doi:10.3390/biomedicines11123291

Journal of Inflammation Research

Dovepress
Taylor & Francis Group

Publish your work in this journal

The Journal of Inflammation Research is an international, peer-reviewed open-access journal that welcomes laboratory and clinical findings on the molecular basis, cell biology and pharmacology of inflammation including original research, reviews, symposium reports, hypothesis formation and commentaries on: acute/chronic inflammation; mediators of inflammation; cellular processes; molecular mechanisms; pharmacology and novel anti-inflammatory drugs; clinical conditions involving inflammation. The manuscript management system is completely online and includes a very quick and fair peer-review system. Visit http://www.dovepress.com/testimonials.php to read real quotes from published authors.

Submit your manuscript here: https://www.dovepress.com/journal-of-inflammation-research-journal